ALGERIAN PEOPLE'S DEMOCRATIC REPUBLIC

Ministry of Higher Education mud Scientific Research

Serial Number: …/2024

University of Kasdi Merbah Ouargla

Faculty of Hydrocarbons, Renewable Energies, Earth, and Universe Sciences.

Department of Hydrocarbon Drilling Oil Mechanics.

THESIS

To obtain the Master's Degree

Option: Drilling

-Title-

Simulation of drilling mud flow in elbow

Presented by :

Ayoub Bendania & Said Belkacem & Youcef Sobhi

Publicly defended on: 16/06/2024

Before the Jury:

President:	Chaich Zieneb	– MCB	Kasdi Merbah Ouargla University
Examiner:	Hadjab Riad	– MCB	Kasdi Merbah Ouargla University
Supervisor:	Hadjadj Souad	– MCB	Kasdi Merbah Ouargla University

The Academic Year 2023/2024

Abstract:

This work aims to make a simulation of the steady, forced, and incompressible flow in the long radius, 90° elbow, using drilling mud, which is considered a pseudoplastic (non-Newtonian fluid), obeyed by the power law, in a laminar and turbulent regime, in order to better understand the hydraulic and thermal behavior of this fluid, as well as the phenomenon known as pressure drop in this area. The simulation program solved the energy balance composed by the differential equations using the Ansys Fluent 2024R1.

The objective of this study is to understand the hydrodynamic and thermal behavior of fluid inside the elbow as well as the phenomenon of pressure drop with a change in the Reynolds number.

The obtained results show that the pressure loss is influenced by the flow regime, and the equation for calculating these losses must be suitable for the type of fluid used.

Keywords: Elbow, non-Newtonian fluid, power law, pressure drop, turbulent.

ملخص :

يهدف هذا العمل إلى محاكاة جريان منتظم، قصري وغير قابل للانضغاط في كوع 90° طويل. سائل الحفر المستعمل يصنف كسائل بسودوبلاستيك غير نيوتوني يخضع لقانون القوة. التدفق صفحي ومضطرب. حل المعادلات التفاضلية من الدرجة الثانية التي تحكم توازن الطاقة باستعمال برنامج المحاكاة.ansys fluent 2024R1

الهدف من هذه الدراسة فهم السلوك الديناميكي والحراري لسائل الحفر داخل الكوع بالإضافة إلى فهم ظاهرة إنخفاض الضغط. من الملاحظ التأثير المباشر لسرعة السائل على ضياع طاقة التدفق في الكوع. إضافة الى ان التوافق بين معادلة الحساب و نوع السائل حتمية لحساب هذا الضياع.

الكلمات المفتاحية : الكوع، سائل غير نيوتوني ، قانون القوة ، انخفاض الطاقة، تدفق مضطرب.

Résumé :

Ce travail étudie une simulation d'un écoulement permanent, forcé et incompressible dans un coude 90°, rayon long. Le fluide de forage utilisé est pseudo-plastique, obéit par la loi de puissance. L'écoulement étudié selon deux régimes, laminaire et turbulent. La résolution du bilan énergétique, géré par des équations différentielles du second ordre est effectuée par le code CFD, Ansys fluent 2024R1.

Le but de cette étude est de comprendre le comportement hydrodynamique et thermique du fluide à l'intérieur du coude ainsi que de comprendre le phénomène de chute de pression avec le changement du nombre de Reynolds.

Les résultats obtenus montrent que le régime d'écoulement ainsi que la vitesse du fluide influent sur la dégradation de pression (d'énergie) et la convenabilité entre l'équation de calcul et le type du fluide utilisé est indispensable.

Mots clés : Le coude, Fluide non newtonien, la loi de puissance, chute de pression, Écoulement turbulent.

ACKNOWLEDGEMENT

First and foremost, we thank God for the strength and patience He has given us to overcome all difficulties.

We express our utmost gratitude to our dear professor Hadjadj Souad for her dedication to the success of this work

Next, we extend our thanks to the members of the examination jury, as well as the administrative staff, for their

kindness. We also thank the engineers, technicians.

We mustnot forget to express our gratitude to the

director who provided us with the opportunity to

undertake the internship,bridging the gap between

the theoretical knowledge acquiredat university and

the practical application in the company, as well as

working on the subject of the final thesis.

Once again, a big thank you to everyone.

Dedication:

I have the great honor to dedicate this modest work:

To myself, as a culmination of all the sleepless nights andsacrifices throughout my journey.

To the remarkable woman who has endured so much to shape me into who I am, who gives me hope to live, and the strength to pursue my dreams and succeed. To the one woman in my life,my beloved mother

To my dear father for his sacrifices in making my wishes cometrue, and for all his prayers that have provided me with support and encouragement.

To my dear sisters and my dear brother, who have always supported me financially and emotionally at every moment,without expecting anything in return.

To all those who have wished me success and happiness

Bendania Ayoub

Dedication:

I dedicate this humble work to:

To my dear parents, as a sign of my gratitude for their patience, sacrifices and support throughout my studies. Thank you, Dear Mom, thank you, dad.

To my dear sisters and brothers, who have been a source of inspiration and courage for me.

To all my friends, with whom I shared my best moments.

For all my teachers since my first years of study.

To everyone who knew me, both closely and from afar.

Said Belkacem

Dedication:

I would like to express my deepest gratitude and dedicate this thesis to the following individuals who have been instrumental in my academic journey:

To my beloved mother and father and grandmother, your unwavering love, support and encouragement have been my guiding light throughout this entire endeavor. Your sacrifices and belief in me have inspired me to pursue my dreams relentlessly. This accomplishment is as much yours as it is mine.

To my partners Ayoub and said, thank you for all your effort and sincerity. I was honored to work with you.

To my family, thank you for your endless support. Your words of encouragement have been constant source of motivation during challenging times. I am blessed to have such a loving and supportive family by my side.

Lastly, to all my friends, both near and far, thank you for your unwavering support and companionship

Youcef Sobhi.

Symbol	Meaning	Unit
C_p	Specific heat at constant pressure	[J/Kg. K]
$C_{1\varepsilon}, C_{2\varepsilon}$	Adjustable constants	
D	Diameter	[m]
f	Friction factor	
K	Consistency index	[Pa.s^n]
k	Turbulent kientic energy	[J]
MW	Mud weight	[ppg]
n	Behavior Index	
P	Pressure	[Pa]
R_e	Reynolds number	
T	Temperature	[K]
T_0	Initial temperature	[K]
T_w	Wall temperature	[K]
u,v,w	Velocity field components	[m.s^{-1}]
$\overline{u}, \overline{v}, \overline{w}$	The components of the average velocity	[m.s^{-1}]
x,y,v	Cartesian Coordinates	[m]
V	Velocity	[m.s^{-1}]
V_{avg}	Average velocity	[m.s^{-1}]
dV	Velocity difference between two adjacent	[m.s^{-1}]
dr	Distance between the two layers	[m]
μ	viscosity	[Pa.s]
μ_a	Viscosity apparent	[Pa.s]
μ_t	Eddy viscosity	[Pa.s]
Z	loss coefficient	
ΔP_L	Linear pressure loss	[Pa]
ΔP_S	Singular pressure loss	[Pa]
$\dot{\gamma}$	Shear rate	[s^{-1}]
τ	Shear stress	[Pa]
$\sigma_\varepsilon, \sigma_k$	adjustable constants	
ρ	Density	[kg.m^{-3}]
Γ_T	Turbulent diffusivity	[W/m.K]
ϵ	Turbulent dissipation rate	[m^2 s^{-3}]

ε	Dissipation rate	[m^2 s^{-3}]
3D	Tridimensional	
FVM	Finite volume method	
CFD	Computational dynamic fluids	

ε	Dissipation rate	[m^2 s^{-3}]

INTRODUCTION

Elbows serve as vital components within the fluid management systems of drilling rigs, playing a crucial role in ensuring the safe and efficient movement of drilling fluids. The meticulous selection, installation, and maintenance of these fittings are imperative for the overall performance and safety of drilling operations. Typically, elbows are employed to alter the direction of the flow of drilling fluid or other substances.

In drilling rigs, elbows are frequently fabricated from high-strength, corrosion-resistant materials such as steel, stainless steel, or specialized alloys to endure the demanding conditions and elevated pressures encountered. These components are designed to be robust and capable of handling the high-pressure and high-volume flow characteristic of drilling mud and other fluids.

This study concerns the steady forced, and incompressible flow in the 90° elbow using pseudoplastic non-Newtonian fluid, obeyed by the power law, in a laminar and turbulent regime, to better understand the hydraulic and thermal behaviour of this fluid as well as the phenomenon known as pressure drop in this area.

The flow is simulated numerically in three dimensions by the finite volume method, using the Ansys Fluent 24 R1 code for the resolution of the energy balance composed of second-order differential equations.

This work includes three chapters. The first chapter provides an overview of drilling fluids, their rheology, and the types of elbows used in drilling fields. The second chapter contains geometric, mathematical, and numerical modelling techniques. The third chapter discusses the results obtained from the modelling studies and their interpretations.

CHAPTER I : GENERALITY

This chapter includes information related to fluid flow and rheology in order to identify and explain the phenomena associated with flow in bends or elbows.

I.1   Rheological Characteristics:

Rheology is the discipline of fluid mechanics which studies relationship between fluid deformation and stress. One goal of rheology is to obtain constitutive equations by which stresses may be computed from deformation rates. For simplicity, fluids may be classified into rheological types in reference to the simple shear flow. [1]

At a given temperature and pressure, fluids are characterized by:

- Their behavior under transient conditions, as manifested by their response time to changed conditions of flow.
- Their behavior in laminar flow, characterized by their experimental flow curve, or rheogram. The constant coefficients of the equation of flow represented by this curve are rheological parameters, specific to the particular fluid.

If the flow is laminar, the equation of flow relates the shear stress τ with the shear rate $\dot{\gamma}$. For a given fluid, it varies with temperature and pressure.

- A shear rate such that:

$$\dot{\gamma} = \frac{dV}{dr} = \frac{\text{Velocity difference between two adjacent layers}}{\text{distance between the two layers}} \qquad (I.1)$$

the dimension $\dot{\gamma}$ is an inverse time [s^{-1} or 1/s].

A shear stress, which is the force per unit area of the laminar layer inducing the shear. τ has the dimensions of pressure. *It* is often expressed in [lb/100 ft^2], [lb force/100 ft^2] or, in the International System of Units (SI) in Pascal [Pa]. [2]

I.2   Non-Newtonian fluids:

Non –Newtonian fluids are those fluids which do not obey Newton's law of viscosity and the relation between shear stress and rate of shear strain is non-linear. These include paints,

coaltar, polymers, lubricants, plastics, printer ink and molecular materials and drilling mud etc. [3]

The ratio of shear stress to shear rate is often called the apparent viscosity to emphasize the distinction from Newtonian behavior. Purely viscous, time-independent fluids, for which the apparent viscosity may be expressed as a function of shear rate, are called generalized Newtonian fluids. [1]

The apparent viscosity μ_a is defined by the equation :

$$\mu_a = \frac{\tau}{\dot{\gamma}} \qquad (I.2)$$

μ_a has the dimensions of viscosity. In the SI system, it is expressed in pascal-second [Pa. s]. The unit which is usually employed is its sub-multiple - the millipascal-second [mPa. s]. It is equal to the centipoise [cP].

It is often necessary to consider the shear stress, shear rate and apparent viscosity at the wall of the channel where the fluid is moving.

Their behavior at rest, as manifested by gel formation after a certain period of time, for thixotropic fluids. [2]

Non-Newtonian fluids include those for which a finite stress τ_y is required before continuous deformation occurs; these are called yield-stress materials. The Bingham plastic fluid is the simplest yield-stress material, its rheogram has a constant slope μ_∞, called the infinite shear viscosity: (Fig I.1).

$$\tau = \tau_y + \mu_p \dot{\gamma} \qquad (I.3)$$

Highly concentrated suspensions of fine solid particles frequently exhibit Bingham plastic behavior.

Shear-thinning fluids are those for which the slope of the rheogram decreases with increasing shear rate. These fluids have also been called pseudoplastic (Fig I.1), but this terminology is outdated and discouraged. Many polymer melts and solutions, as well as some solids suspensions, are shear-thinning. Shear-thinning fluids without yield stresses typically obey a power law model over a range of shear rates. Shear-thinning power law fluids with yield

stresses are sometimes called Herschel-Bulkley fluids. Numerous other rheological model equations for shear-thinning fluids are in common use, as casson and Robertson − stiff.

Dilatant, or shear-thickening, fluids show increasing viscosity with increasing shear rate. Dilatancy is rare observed only in certain concentration ranges in some particle suspensions.
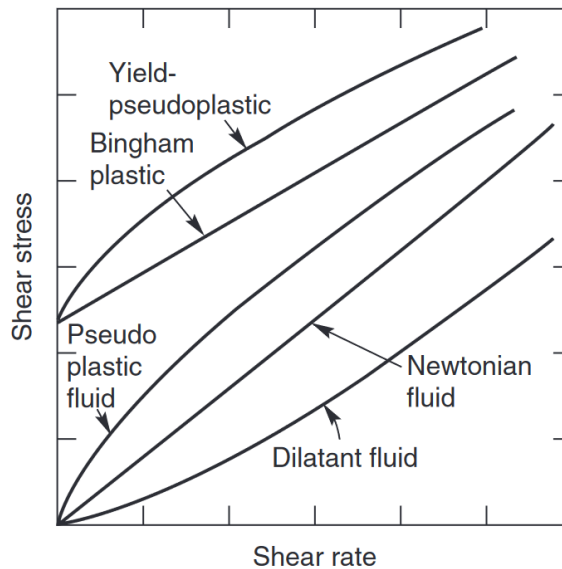
Figure I.1: Types of time-independent flow behavior [4]

Time-dependent fluids are those for which structural rearrangements occur during deformation at a rate too slow to maintain equilibrium configurations. As a result, shear stress changes with duration of shear. Thixotropic fluids, such as mayonnaise, clay suspensions used as drilling muds, and some paints and inks, show decreasing shear stress with time at constant shear rate.

Rheopectic behavior is the opposite of thixotropy. Shear stress increases with time at constant shear rate. Rheopectic behavior has been observed in bentonite sols, vanadium pentoxide sols, and gypsum suspensions in water as well as in some polyester solutions. (Fig I.2)

Viscoelastic fluids exhibit elastic recovery from deformation when stress is removed. Polymeric liquids comprise the largest group of fluids in this class. A property of viscoelastic fluids is the relaxation time, which is a measure of the time required for elastic effects to decay. Viscoelastic effects may be important with sudden changes in rates of deformation, as in flow

startup and stop, rapidly oscillating flows, or as a fluid passes through sudden expansions or contractions where accelerations occur. In many fully developed flows where such effects are absent, viscoelastic fluids behave as if they were purely viscous. In viscoelastic flows, normal stresses perpendicular to the direction of shear are different from those in the parallel direction. [1]
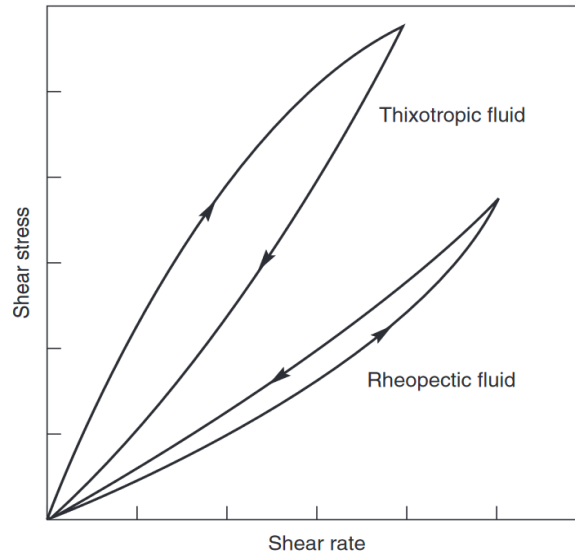
Figure I.2: Types of time dependent flow behavior [4]

I.3   Pseudo-plastic or power-law fluids:

Pseudo-plastic fluids, like Newtonian fluids, will flow under any applied stress, however small. But, as distinct from Newtonian fluids, the shear stress is not proportional to the shear rate, but to its **n^{th}** power; hence the name power-law fluids.

$$\tau = K\dot{\gamma}^n \tag{I.4}$$

where **K** is the consistency index in [Pa s^n] or in [lb s^n/100ft^2], and **n** is the dimensionless flow behavior index, which is unity or smaller than unity. If **n = 1**, the equation becomes identical with the equation of flow of a Newtonian fluid having the viscosity K. The following graphs shown in (Fig I.3) are flow curves of power-law fluid in Cartesian and logarithmic coordinates respectively.

In logarithmic coordinates, the flow curve is a straight line, the equation of which is:

$$y = \log K + nx \tag{I.5}$$

Where: $y = \log\tau$ and $x = \log\dot\gamma$
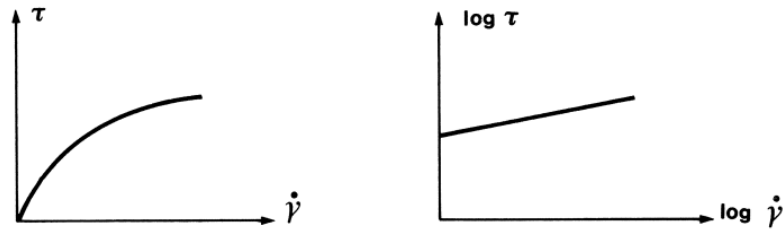
Figure I.3: Flow curves of power-law fluid in Cartesian and logarithmic coordinates [2]

Thus, the flow behavior index *n* represents the slope of this line, while the fluid consistency index *K* is given by the intersection of the flow curve with the axis at $\dot\gamma = 1$:

The determinations made in a six-speed Fann viscometer (or, if this instrument is not available, in a two-speed Fann viscometer, using also **g₀**, which is considered to represent a determination at 3 rpm) are plotted, as a rheogram, on log-log paper, shear rates in [s⁻¹] being plotted on the abscissa, shear stresses (in lb/l00 ft²) on the ordinate (Fig I.4). [2]
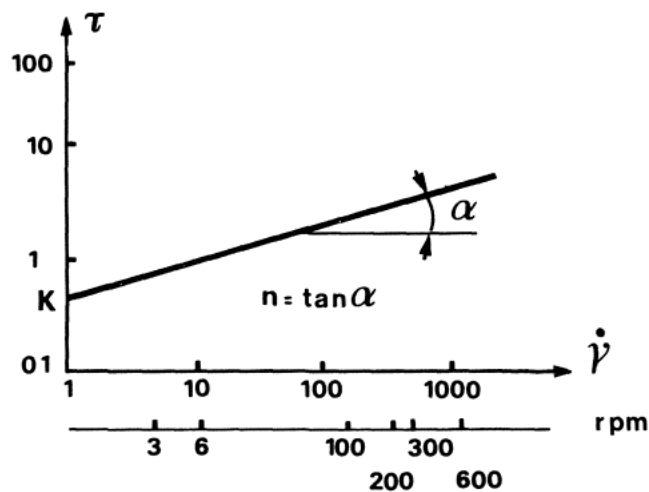
Figure I.4:Parameters of power-law fluid rheological [2]

$$n = \frac{\log\tau \; / \; \tau'}{\log\dot\gamma \; / \; \dot\gamma'} \qquad (I.7)$$

If $\dot\gamma = 2\dot\gamma'$, we have:

$$n = \frac{\log \tau / \tau'}{\log 2} = \frac{\log \theta / \theta'}{\log 2} = \log \frac{\theta}{\theta'} \tag{I.8}$$

from equation (I.4), if $\dot{\gamma}=1$; $k= \tau_1$.

I.4 Flow regime and Reynolds Number:

The Reynolds number is a dimensionless, empirically-deduced parameter. The significance of the Reynolds number is in its use as a correlation parameter: different fluids with different properties exhibit similar flow characteristics at the same Reynolds number.

The major use of the Reynolds number is the determination of flow regime. Generally, the flow regime of a liquid changes from laminar to turbulent at a fairly well-defined Reynolds number (Re) value. [5]

$$R_e = \frac{\rho V_{avg} D}{\mu} \tag{I.9}$$

With:

ρ: the fluid density

V_{avg}: average velocity of fluid

D: hydraulic diameter

μ : dynamic viscosity

Or, in oilfield units : [5]

$$R_e = \frac{15.47 \times MW \times V_{avg} \times D}{\mu} \tag{I.10}$$

MW: Mud Weight. (ppg).

Reynolds observed that water changed from laminar flow to turbulent flow at a Reynolds number of approximately 2000.

It is apparent that Equation (I.9 – I.10) is not valid for a non-Newtonian fluid because non-Newtonian fluids do not have an absolute viscosity; the viscosity varies with shear rate. [5]

For laminar flow, the apparent viscosity has the property that it is the viscosity of a Newtonian fluid having the same flow characteristic as the non-Newtonian fluid when subjected to the same value of wall shear stress. In particular, this corresponds to the same

volumetric flow rate for the same pressure gradient in the same pipe. This suggests that μ_a might be a useful quantity for correlating flow rate-pressure gradient data for non-Newtonian flow in pipes. This is found to be the case and it is on μ_a that a generalized Reynolds number (Re_{gen}) is based:[6]

$$Re_{gen} = \frac{\rho V_{avg} D}{\mu_a} \qquad (I.11)$$

The power law model is very popular for representing the viscosity of a wide variety of non-Newtonian fluids because of its simplicity and versatility. However, extreme care should be exercised in its application, because any application involving extrapolation beyond the range of shear stress (or shear rate) represented by the data used to determine the model parameters can lead to misleading or erroneous results. Both laminar and turbulent pipe flow of highly loaded slurries of fine particles, for example, can often be adequately represented by either of these two models over an appreciable shear rate range. [7]

The apparent viscosity for the power law fluid is a same in all flow regime in pipe: [2]

$$\mu_a = K \left(\frac{8V}{D} \frac{3n+1}{4n} \right)^{n-1} \qquad (I.12)$$

Reynolds number for the power law fluid is defined as: [2]

$$R_e = \frac{V^{n-1} D^n \rho}{K 8^{n-1}((3n+1)/4n)^n} \qquad (I.13)$$

Another value used to determine flow regime is the critical velocity. The critical velocity is calculated by solving the Reynolds-number equation for velocity at the Reynolds-number value at which turbulence begins. called the critical Reynolds number ($Re = Re_c = 3470 - 1370n$). Thus. from Equation (I.13), the critical velocity of a power law fluid is [5]:

$$V_c = \left(\frac{(3470 - 1370n) K 8^{n-1}((3n+1)/4n)^n}{D^n \rho} \right)^{\frac{1}{2-n}} \qquad (I.14)$$

I.5   Pressure Loss:

Pressure loss, also known as head loss, refers to the energy loss experienced by a fluid as it flows through a system. This loss arises due to two main factors:

Friction: The fluid experiences friction as it rubs against the walls of the system, dissipating energy. This friction loss is proportional to the length of the flow path and the fluid velocity.

Obstacles: Components like elbows, bends, valves, and changes in pipe diameter act as obstacles, creating resistance to the flow and causing additional energy loss. This loss depends on the geometry and type of the obstacle.

Pressure loss can be expressed as a pressure drop. [8]

I.5.1   Linear pressure loss:

This loss occurs uniformly along the entire length of the flow path due to friction against the channel walls. The amount of friction loss depends on the fluid's viscosity, velocity, and the surface roughness. It is proportional to the length of the circuit and the velocity of the Newtonian fluid. [8]

$$\Delta P_L = f\frac{\rho L V^2}{2D} \tag{I.15}$$

With:

ΔP_L: Linear pressure loss

f: Friction factor

L: Length of the circuit

D: Diameter of the pipe

ρ: Density of the fluid

V: Velocity of the fluid

For power law fluid : [2]

❖   Laminar flow : Re < 3470-1370n

$$\Delta P = \frac{32 \, L \, \mu_a \, V}{D^2} \frac{3n + 1}{4n} \qquad (I.16)$$

❖   Turbulent flow : Re ≥ 3470-1370n

$$\Delta P = \left(\frac{2cL \, \rho^{1-b} V^{2-b}}{D^{1+b}} \right) \left(\mu_a{}^b \left(\frac{3n + 1}{4n} \right)^b \right) \qquad (I.17)$$

Where :

$$c = \frac{\log n + 2{,}5}{50} \; ; \quad b = \frac{1{,}4 - \log n}{7} \; ; \quad f = \frac{c}{Re^b} \qquad (I.18)$$

f is the coefficient of head-pressure loss.

❖ Determining the Friction Factor:

The Darcy friction factor depends on the Reynolds number (Re) and the relative roughness of the elbow's inner surface. It can be determined using Moody charts (Figure I.5) or explicit equations like the Blasius equation or Colebrook equation or Lea equation. [9]
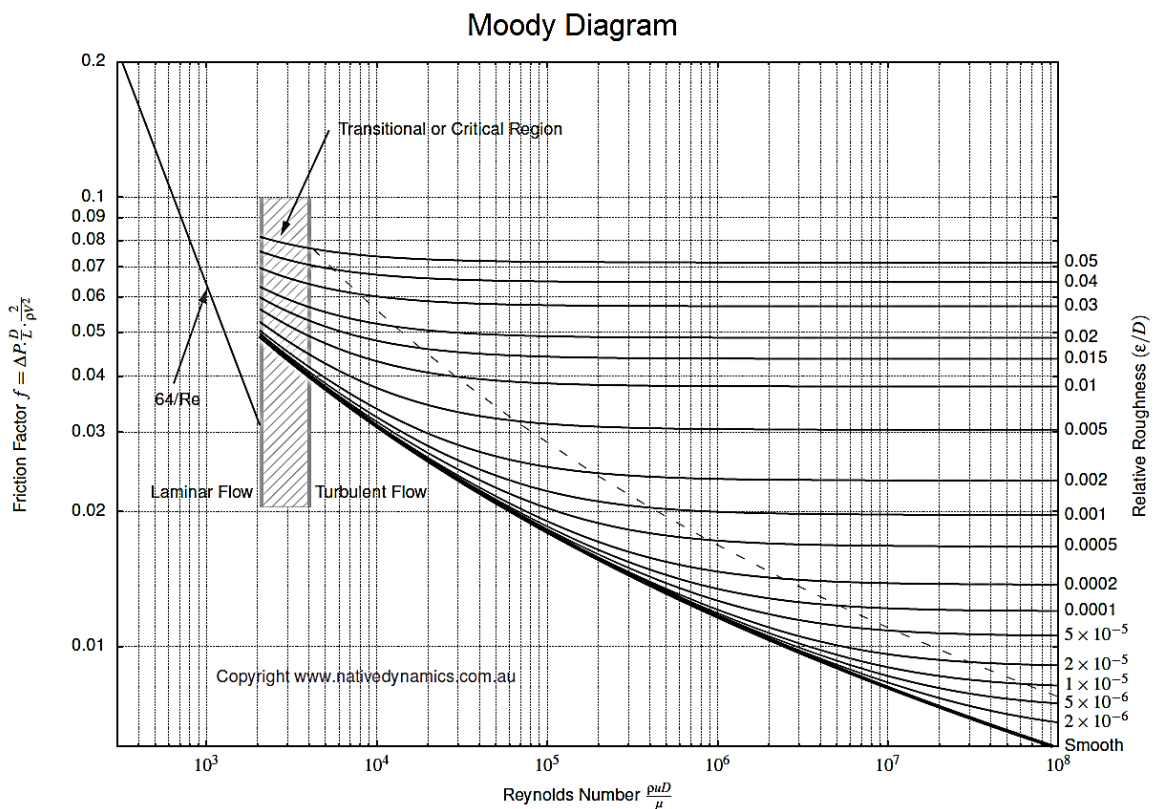

Figure I.5: Moody Chart (Newtonian Fluid) [9]

- ▪ Laminar Flow: [10]

In the laminar flow regime, the Darcy Equation may be used to determine the friction factor.

For Re <2300

$$f = \frac{64}{Re} \qquad (I.19)$$

- ▪ Turbulent Flow: [10]

❖ Blasius formula: $3000 \leq Re \leq 10^5$

$$f = \frac{0.3164}{Re^{0.25}} \qquad (I.20)$$

❖ Colebrook-white formula: $Re > 10^5$

$$\frac{1}{\sqrt{f}} = 2\log_{10}(Re \times \sqrt{f}) - 0.8 \qquad (I.21)$$

❖ Lea formula: $4000 \leq Re \leq 4 \times 10^5$

$$f = 0.0072 + \frac{0.3164}{Re^{0.25}} \qquad (I.22)$$

For Power Law fluids, from the Blasius relationship is of the form: [5]

$$f = yRe^{-z} \qquad (I.23)$$

y and z show some dependence on the flow behavior index n. The experimental results of Dodge and Metzner, analyzed by Schuh, yield expressions for y and z.

$$y = \frac{\log n + 3.93}{50} \qquad (I.24)$$

$$z = \frac{1.75 + \log n}{7} \qquad (I.25)$$

The von Karman relationship for Power Law fluids investigated by Dodge and Metzner:

$$\frac{1}{\sqrt{f}} = \frac{4}{75n}\log\left(\text{Re}.f^{1+n/2}\right) - \frac{0.4}{n^{1.2}} \qquad\qquad (I.26)$$

Figures I.6-7 show the Blasius and von Karman correlations for various Power Law fluids. A line is also drawn to represent the laminar flow regime.
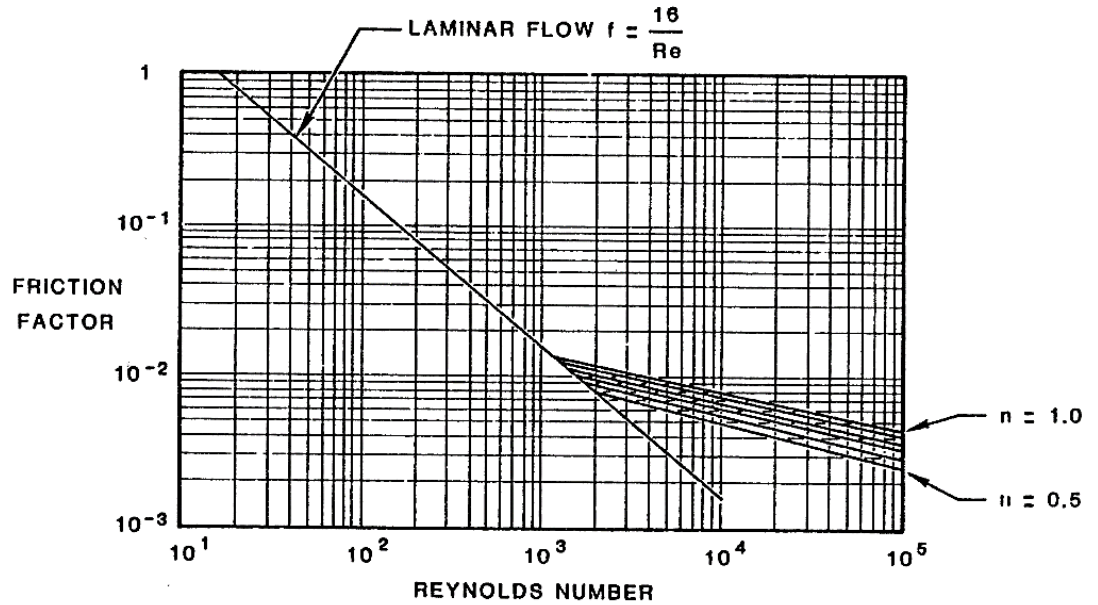

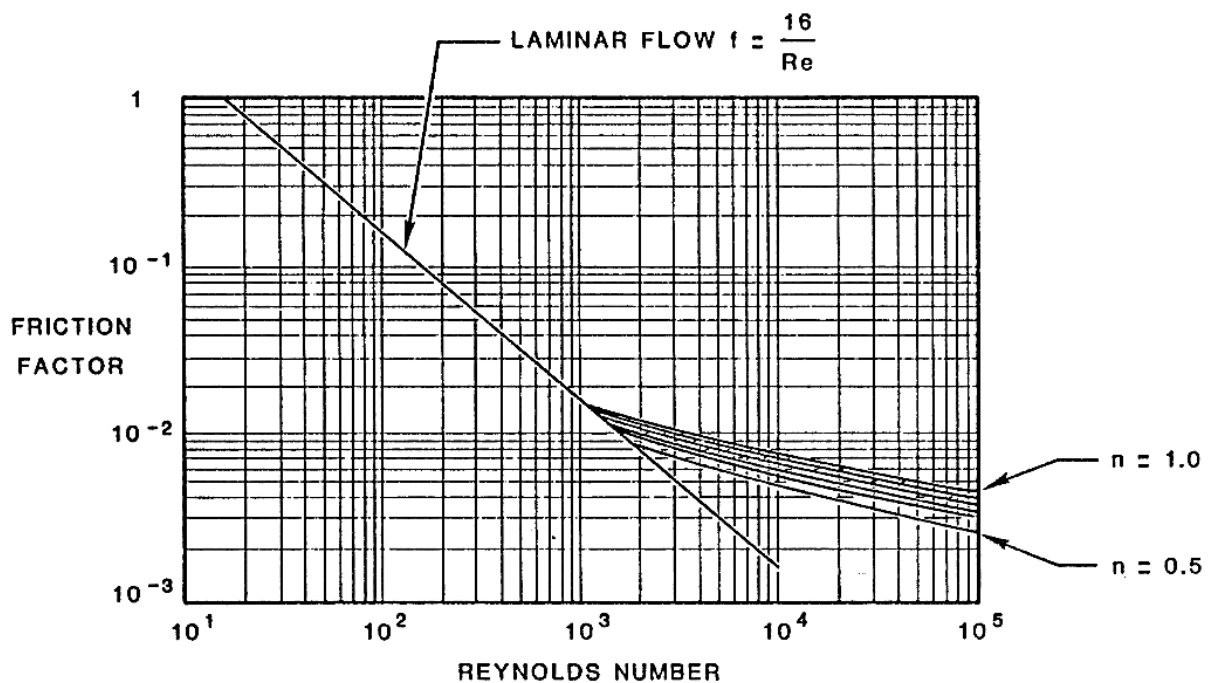Figure I.6: Blasius Correlation for Various Power Law Fluids [5]

Figure I.7: Von Karman Correlation for Various Power Law Fuids [5]

I.5.2 Singular pressure loss:

This loss occurs localized at specific points within the system due to obstacles like elbows, valves, and expansions/contractions. It is calculated using empirical coefficients specific to each type of obstacle. [11]

$$\Delta P_S \;=\; Z\frac{\rho V^2}{2} \qquad\qquad (\text{I. }27)$$

With

ΔP_S: Singular pressure loss

Z: Loss coefficient

ρ: Density of the fluid

V: Velocity of the fluid

I.6 Elbow:

Elbow is a pipe fitting which is used as a connection point between two lengths of pipes to produce a change in the direction of flow in the pipe. Elbows are also commonly referred as bends. [12]

This is available many in different angles – like 45°, 90°, and some special 22.5° angles – by cutting the standard available elbow (45°, 90°) in another degree as well, as per user requirement. Elbow is available in two radius lengths, such as short radius (45°) and long radius (90°) elbow. 90° elbow (90° ell) are also called quarter bend elbow also, because the flow is redirected to one quarter of 360° that means 90. But due to sudden redirect of fluid flow rate and pressure within the pipe, the elbow will be dropped. That is only one disadvantage of using the elbow in industries pipeline. [13]

I.6.1 Types of elbows:

The types of pipe elbow categorized on the base for the following point some of them are described below. (Fig I.8). [13]

On the base of end connection types:

- ✓ Bevel end connections types
- ✓ Plain end connection types
- ✓ Threaded end connection types

➢ On the base of end joint connection with pipes

- ✓ Socket welds joint
- ✓ Butt welds joints
- ✓ Threaded joint
- ✓ Male female connections

➢ On the base of radius types

- ✓ Short radius Elbow
- ✓ Long radius type

➢ On the base of pipe elbow angles standards elbow or non-standard

- ✓ 45° bend pipe fitting
- ✓ 90° bend pipe fitting
- ✓ 60° bend pipe fitting
- ✓ 120° bend pipe fitting
- ✓ 180° bend pipe fitting
- ✓ 22° bend (Non standards bend)

Types of Pipe Elbows as per End Connection
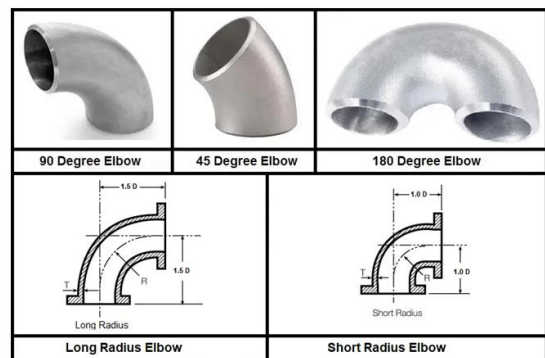
Types of piping elbows depending on bend radius and angles

Figure I.8: Types of elbows [14]

I.6.2 Pressure loss in elbow:

The pressure loss in pipe bends may be thought of as made up of three components. One component is the pressure loss due to ordinary surface friction that corresponds to fully developed flow in a straight pipe having the same length as the centerline of the bend. A second component is due to a twin - eddy secondary flow superimposed on the main or primary flow due to the combined action of centrifugal force and frictional resistance of the pipe walls. A third component is due to separation of the main flow from the inner and outer radius of the bend and subsequent expansion of the contracted stream. For bends of short radius of curvature, flow separation and secondary flow dominate. For bends of long radius of curvature, ordinary surface friction and secondary flow prevail. (Fig I.9)
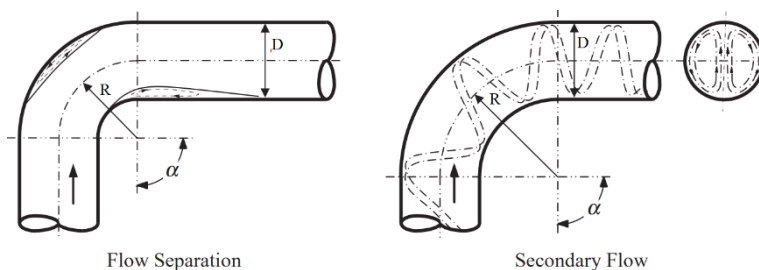

Flow Separation   Secondary Flow

Figure I.9: Curved pipe flow [15]

The bend radius ratio (R/D) is defined as the ratio of the centerline radius of the bend to the inside diameter of the pipe. In this context, a bend of radius ratio (0.5) represents a bend with a sharp (zero radius) inner corner and an outer bend radius of (1). At the extreme is a miter bend in which two pipes are joined together in a sharp angle without any rounding at the plane of intersection. The rounding of the corner at the inner wall, or simply beveling the corner, greatly attenuates the separation and reduces the pressure loss. At the opposite extreme, bend losses, excluding friction losses, are at a minimum when the bend radius ratio is at a maximum. (Fig I.9)

A bend must always be considered with relation to the straight pipes, or tangents, connected to its ends. This brings about experimental difficulties. Whatever the velocity distribution may be at the upstream end, the downstream length must be sufficient for the gradual adjustment of the distribution until it regains a normal velocity profile. An example of

the measured pressure distribution along a bend is shown in (Fig I.10). In this bend of circular cross section, a marked increase in pressure along the outer wall is accompanied by a corresponding decrease in pressure along the inner wall. The bend loss is found by measuring the pressure difference between static pressure taps located just before the bend and taps located 40 diameters or so down-stream of the bend and then subtracting the ordinary friction loss for developed flow in straight pipe between the two taps. Because the friction loss over this distance may be many times the bend loss, particularly for small deflection angles, the pressure loss is often the difference between two large values. Very careful and accurate measurements are required under these conditions to obtain accurate results.

Because of its considerable importance in the design and analysis of fluid machinery and piping systems, a vast amount of experimental and theoretical data on flow through bends has been reported over the past century. However, a review of the literature shows wide variations in loss coefficients quoted by the various investigators. Because actual details of their test conditions are often lacking, it is not possible to correct their results to provide meaningful data. In any case, all investigators report that bend loss is a strong function of friction factor. Many investigators go so far as to characterize bend loss as a direct function of friction factor.

The Dean number, a dimensionless number giving the ratio of the viscous force acting on a fluid in a curved pipe to the centrifugal force, has frequently been employed in the study of flow in curved pipes and channels. Nonetheless, the authors did not employ the Dean number to aid (or hamper) their formulation of bend loss coefficient.
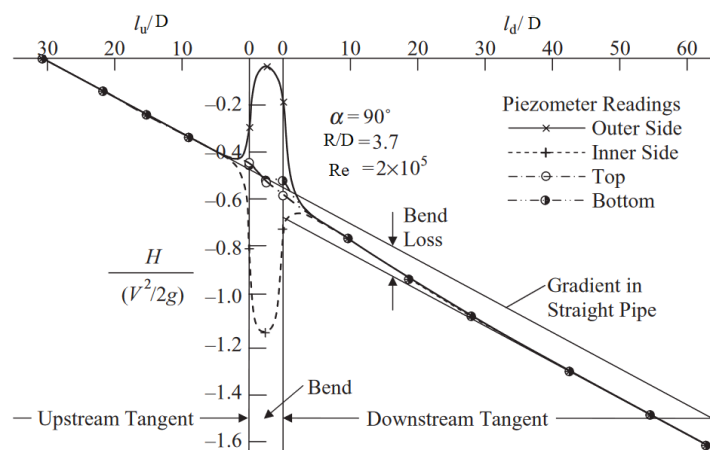

Figure I.10: Static pressure distribution in the neighborhood of a bend with long tangents [15]

Investigators agree that the loss coefficient of elbows and curved pipe is practically a direct function of friction factor. The friction factor in smooth - walled tests can be fairly accurately predicted as a function of Reynolds number. Accordingly, most experimental and theoretical data have been for smooth – walled bends. There are very little useful data on rough – walled bends. The experimenters often used artificially roughened pipe and actual surface roughness was usually not reported.

For curved pipe, the effects of surface friction, secondary flow, and flow separation can be rationally divided into three distinct effects as illustrated in (Fig I.11). The lower region represents ordinary surface friction loss as in a straight stretch of pipe equal to the centreline distance of the bend. The mid - and upper regions can be attributed to secondary flow loss and flow separation loss, respectively.
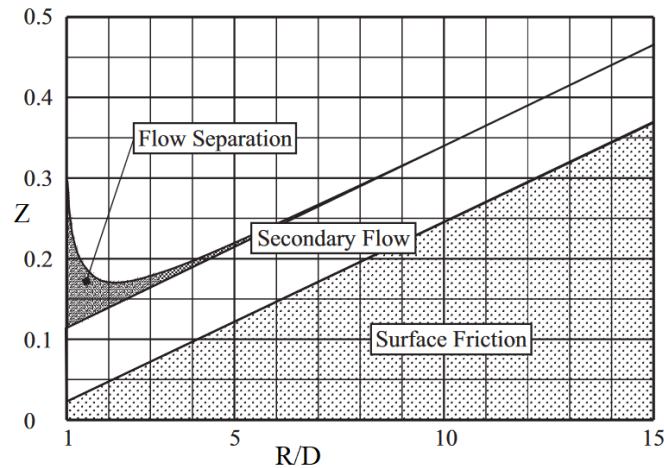

Figure I.11: Distinct effects of surface friction, secondary flow, and flow separation [15]

Employing smooth- walled test data, the author developed an empirical equation for circular bends for R/D equal to or greater than 0.5, and for bend angle α from zero to π /2 (180°)

$$Z = f\alpha \frac{R}{D}(0,1 + 2,4f)\sin(\alpha/2) + \frac{6,6f\sqrt{\sin(\alpha/2)} + \sin(\alpha/2)}{(R/D)^{4\alpha/\pi}} \qquad (I.28)$$

The first term in this equation represents surface friction loss, the second term represents secondary flow, and the third term represents flow separation. Note that Equation (I.28) essentially encompasses the entire range of elbow and pipe bend configurations.

To obtain loss coefficient Z in the case of turbulent flow in the transition zone, or for other than clean steel pipe, simply adjust the tabulated values as follows:

$$Z = \frac{f}{f_t} Z_t \qquad (I.29)$$

where f is friction factor at the flow condition of interest, and f_t and Z_t are obtained from Tables. This method is reasonable because, as evident in Equation (I.28), the loss coefficient for curved bends is very nearly a direct function of friction factor. If greater precision is desired, calculate the loss coefficient directly using Equation (I.28). [15]

CHAPTER II : PROBLEMATIC

II.1 Elbow in drilling Rig:

Elbows are essential components in the fluid management systems of drilling rigs, ensuring the safe and efficient flow of drilling fluids. Proper selection, installation, and maintenance of these fittings are critical to the overall performance and safety of drilling operations. Its typically used to change the direction of the flow of drilling fluid or other substances.

In drilling rig, elbows are typically available in angles such as 45 degrees and 90 degrees come in:

- **Long Radius Elbows**: These have a larger radius compared to standard elbows, providing a smoother change in direction, which can reduce pressure loss and turbulence in the flow.
- **Short Radius Elbows**: These have a tighter turn radius, used where space is limited, but can create more pressure drop and turbulence.

Elbows used in drilling rigs are often made from high-strength, corrosion-resistant materials such as steel, stainless steel, or specialized alloys to withstand harsh conditions and high pressures. They are constructed to be robust and capable of handling the high-pressure and high-volume flow of drilling mud and other fluids. Their essential applications, are:

- **Mud Circulation**: Elbows are used in the mud circulation system of a drilling rig to direct the flow of drilling mud from one part of the system to another.
- **Pipe Systems**: They are integral in the pipe systems on the rig floor and in the derrick, where they help manage the routing of fluids under high pressure. (Fig II.1-2)

Figure II.1: 45° elbows in drilling rig

Figure II.2: 90° elbows in drilling rig

II.2 Physical description:

In order to complete this study, we take 90° elbow long radius from the drilling mud installation. Its Nominal Pipe Size (NPS) is 8'' (203.2 mm), with the center to end length (R) 304,8 mm and the Outer Diameter (OD) 219,1 mm. Pipe lengths in upstream and downstream are 1 m and 2 m, respectively. The positions studied of this elbow are indicated in (Fig II.3).
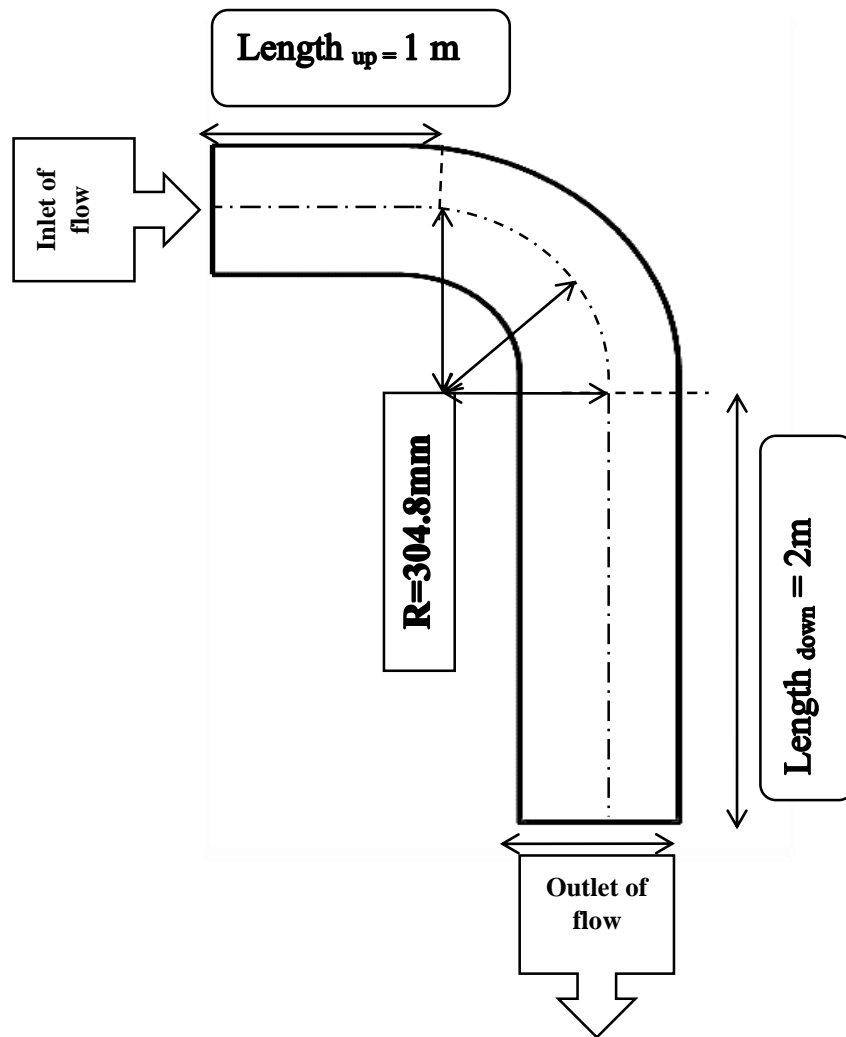
To investigate the behavior of the elbow during drilling mud flow, the pipe assembly including the elbow was segmented into multiple streamlines. The upstream section was divided into two segments at distances of approximately 0.1 m from the pipe inlet and 1.0 m from the pipe outlet, respectively.
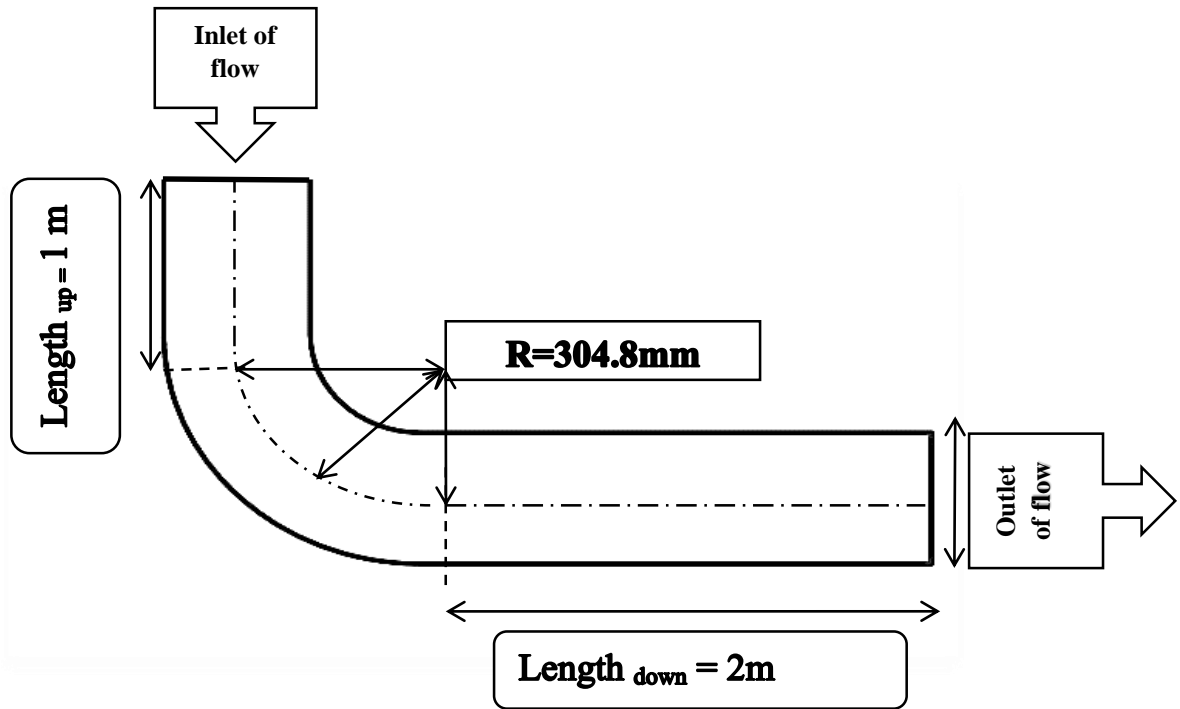
a-first case
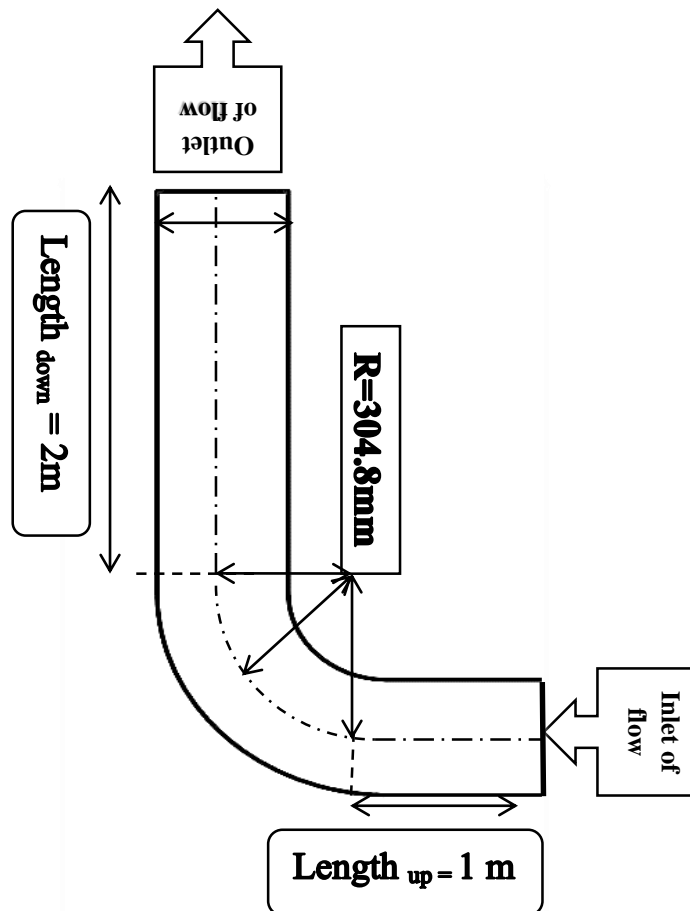
b- second case

c- third case

Figure II.3: Elbows positions studied vertical projection, a-first case, b-Second case, c-
third case

Hypothesis:

- The flow is incompressible, steady.

- The fluid is non-Newtonian pseudo plastic, obeying Power's law

- All walls are considered impermeable and isothermal.

- The thermo-physical parameters (density, thermal conductivity and mass heat capacity) are constant, calculated at a reference temperature T_{ref} or film temperature.

- The heat transfer mode is forced convection

- The viscous dissipations are neglected

II.3 Mathematical formulation:

The energy balance of this flow is governed by the following equations:

II.3.1 laminar flow [16]:

❖ **Continuity equation:**

$$\frac{\partial u}{\partial x} + \frac{\partial v}{\partial y} + \frac{\partial w}{\partial z} = 0 \qquad\qquad \text{(II. 1)}$$

❖ **Momentum Equations:**

$$\rho\left(u\frac{\partial u}{\partial x} + v\frac{\partial u}{\partial y} + w\frac{\partial u}{\partial z}\right) = -\frac{\partial P}{\partial x} + \mu\left(\frac{\partial^2 u}{\partial x^2} + \frac{\partial^2 u}{\partial y^2} + \frac{\partial^2 u}{\partial z^2}\right) \qquad \text{(II. 2. a)}$$

$$\rho\left(u\frac{\partial v}{\partial x} + v\frac{\partial v}{\partial y} + w\frac{\partial v}{\partial z}\right) = -\frac{\partial P}{\partial y} + \mu\left(\frac{\partial^2 v}{\partial x^2} + \frac{\partial^2 v}{\partial y^2} + \frac{\partial^2 v}{\partial z^2}\right) \qquad \text{(II. 2. b)}$$

$$\rho\left(u\frac{\partial w}{\partial x} + v\frac{\partial w}{\partial y} + w\frac{\partial w}{\partial z}\right) = -\frac{\partial P}{\partial z} + \mu\left(\frac{\partial^2 w}{\partial x^2} + \frac{\partial^2 w}{\partial y^2} + \frac{\partial^2 w}{\partial z^2}\right) \qquad \text{(II. 2. c)}$$

❖ **Energy equation**:

$$\rho C_P\left(u\frac{\partial T}{\partial x} + v\frac{\partial T}{\partial y} + w\frac{\partial T}{\partial z}\right) = -\lambda\left(\frac{\partial^2 T}{\partial x^2} + \frac{\partial^2 T}{\partial y^2} + \frac{\partial^2 T}{\partial z^2}\right) \qquad \text{(II. 3)}$$

II.3.2 Turbulent flow:

The k-epsilon ($k-\epsilon$) model for turbulence is the most common to simulate the mean flow characteristics for turbulent flow conditions. It is an Eddy viscosity model which is a class of turbulence models used to calculate the Reynolds stresses.

It is a two-equation model. That means in addition to the conservation equations, it solves two transport equations (PDEs), which account for the historical effects like convection and diffusion of turbulent energy. The two transported variables are turbulent kinetic energy (k), which determines the energy in turbulence, and turbulent dissipation rate (ϵ), which determines the rate of dissipation of turbulent kinetic energy.

Different variations of the k-epsilon model exist such as Standard, Realizable, RNG, etc. each with certain modifications to perform better under certain fluid flow conditions. [17]

When the flow regime becomes turbulent, the velocity, pressure and temperature are considered as random functions in space and time, of which these values instantaneous are broken down into:

$$u = \bar{u} + u'; v = \bar{v} + v'; w = \bar{w} + w'; p = \bar{p} + p'; T = \bar{T} + T'$$

The symbol (¯) represents the statistical average or ensemble average operator and the symbol (´) denotes fluctuations or deviations from these averages.

The previous equations (II.1), (II.2.a), (II.2.b), (II.2.c) and (II.3) are written in the forms following:

❖ **Continuity equation:**

$$\frac{\partial \bar{u}}{\partial x} + \frac{\partial \bar{v}}{\partial y} + \frac{\partial \bar{w}}{\partial z} = 0 \tag{II.4}$$

❖ **Momentum equation:**

$$\rho \left(\bar{u} \frac{\partial \bar{u}}{\partial x} + \bar{v} \frac{\partial \bar{u}}{\partial y} + \bar{w} \frac{\partial \bar{u}}{\partial z} \right) + \rho \left(\frac{\partial \overline{u'u'}}{\partial x} + \frac{\partial \overline{u'v'}}{\partial y} + \frac{\partial \overline{u'w'}}{\partial z} \right)$$

$$= -\frac{\partial \bar{P}}{\partial x} + \frac{\partial}{\partial x} \left(\mu \frac{\partial \bar{u}}{\partial x} \right) + \frac{\partial}{\partial y} \left(\mu \frac{\partial \bar{u}}{\partial y} \right) + \frac{\partial}{\partial z} \left(\mu \frac{\partial \bar{u}}{\partial z} \right) \tag{II.5.a}$$

$$\rho \left(\bar{u} \frac{\partial \bar{v}}{\partial x} + \bar{v} \frac{\partial \bar{v}}{\partial y} + \bar{w} \frac{\partial \bar{v}}{\partial z} \right) + \rho \left(\frac{\partial \overline{v'u'}}{\partial x} + \frac{\partial \overline{v'v'}}{\partial y} + \frac{\partial \overline{v'w'}}{\partial z} \right)$$

$$= -\frac{\partial \bar{P}}{\partial y} + \frac{\partial}{\partial x} \left(\mu \frac{\partial \bar{v}}{\partial x} \right) + \frac{\partial}{\partial y} \left(\mu \frac{\partial \bar{v}}{\partial y} \right) + \frac{\partial}{\partial z} \left(\mu \frac{\partial \bar{v}}{\partial z} \right) \tag{II.5.b}$$

$$\rho \left(\bar{u} \frac{\partial \bar{w}}{\partial x} + \bar{v} \frac{\partial \bar{w}}{\partial y} + \bar{w} \frac{\partial \bar{w}}{\partial z} \right) + \rho \left(\frac{\partial \overline{w'u'}}{\partial x} + \frac{\partial \overline{w'v'}}{\partial y} + \frac{\partial \overline{w'w'}}{\partial z} \right)$$

$$= -\frac{\partial \bar{P}}{\partial z} + \frac{\partial}{\partial x} \left(\mu \frac{\partial \bar{w}}{\partial x} \right) + \frac{\partial}{\partial y} \left(\mu \frac{\partial \bar{w}}{\partial y} \right) + \frac{\partial}{\partial z} \left(\mu \frac{\partial \bar{w}}{\partial z} \right) \tag{II.5.c}$$

We notice that this energy balance resembles that in laminar regime, except the terms:$\overline{u'T'}; \overline{v'T'}$ and $\overline{w'T'}$ called the extra-terms of temperature and the constraints of Reynolds, following:

$$-\overline{\rho u'u'} = 2\mu_T \frac{\partial \overline{u}}{\partial x} - \frac{2}{3}\rho k; \overline{-\rho v'v'} = 2\mu_T \frac{\partial \overline{v}}{\partial y} - \frac{2}{3}\rho k; \overline{-\rho w'w'} = 2\mu_T \frac{\partial \overline{w}}{\partial z} - \frac{2}{3}\rho k \text{ (II. 6)}$$

$$\overline{-\rho u'v'} = \mu_T \left(\frac{\partial \overline{v}}{\partial x} + \frac{\partial \overline{u}}{\partial y}\right); \overline{-\rho u'w'} = \mu_T \left(\frac{\partial \overline{w}}{\partial x} + \frac{\partial \overline{u}}{\partial z}\right); \overline{-\rho v'w'} = \mu_T \left(\frac{\partial \overline{w}}{\partial y} + \frac{\partial \overline{v}}{\partial z}\right); \quad \text{(II. 7)}$$

Where: μ_T is the turbulent viscosity and k is the turbulent kinetic energy.

For turbulent kinetic energy k:

$$\frac{\partial(\rho k u)}{\partial x} + \frac{\partial(\rho k v)}{\partial y} + \frac{\partial(\rho k w)}{\partial z} = \frac{\partial}{\partial x}\left(\frac{\mu_t}{\sigma_k}\frac{\partial k}{\partial x}\right) + \frac{\partial}{\partial y}\left(\frac{\mu_t}{\sigma_k}\frac{\partial k}{\partial y}\right) + \frac{\partial}{\partial z}\left(\frac{\mu_t}{\sigma_k}\frac{\partial k}{\partial z}\right) +$$

$$2\mu_t\left[\left(\frac{\partial \overline{u}}{\partial x}\right)^2 + \left(\frac{\partial \overline{v}}{\partial y}\right)^2 + \left(\frac{\partial \overline{w}}{\partial z}\right)^2 + \left(\frac{\partial \overline{u}}{\partial y} + \frac{\partial \overline{v}}{\partial x}\right)^2 + \left(\frac{\partial \overline{u}}{\partial z} + \frac{\partial \overline{w}}{\partial x}\right)^2 + \left(\frac{\partial \overline{v}}{\partial z} + \frac{\partial \overline{w}}{\partial y}\right)^2\right] - \rho\varepsilon$$

$$\text{(II.8)}$$

Dissipation rate of turbulent kinetic energy:

$$\frac{\partial(\rho \varepsilon u)}{\partial x} + \frac{\partial(\rho \varepsilon v)}{\partial y} + \frac{\partial(\rho \varepsilon w)}{\partial z} = \frac{\partial}{\partial x}\left(\frac{\mu_t}{\sigma_\varepsilon}\frac{\partial \varepsilon}{\partial x}\right) + \frac{\partial}{\partial y}\left(\frac{\mu_t}{\sigma_\varepsilon}\frac{\partial \varepsilon}{\partial y}\right) + \frac{\partial}{\partial z}\left(\frac{\mu_t}{\sigma_\varepsilon}\frac{\partial \varepsilon}{\partial z}\right) +$$

$$C_{1\varepsilon}\frac{\varepsilon}{k}2\mu_t\left[\left(\frac{\partial \overline{u}}{\partial x}\right)^2 + \left(\frac{\partial \overline{v}}{\partial y}\right)^2 + \left(\frac{\partial \overline{w}}{\partial z}\right)^2 + \left(\frac{\partial \overline{u}}{\partial y} + \frac{\partial \overline{v}}{\partial x}\right)^2 + \left(\frac{\partial \overline{u}}{\partial z} + \frac{\partial \overline{w}}{\partial x}\right)^2 + \left(\frac{\partial \overline{v}}{\partial z} + \frac{\partial \overline{w}}{\partial y}\right)^2\right]$$

$$- C_{2\varepsilon}\rho\frac{\varepsilon^2}{k} \qquad\qquad\qquad \text{(II. 9)}$$

Where:

$\mu_t = \rho C_\mu k^2/\varepsilon$ represents eddy viscosity

$\sigma_\varepsilon, \sigma_k, C_{1\varepsilon}$ and $C_{2\varepsilon}$ are adjustable constants

❖ **The Energy Equation :**

$$\rho C_P\left(\overline{u}\frac{\partial \overline{T}}{\partial x} + \overline{v}\frac{\partial \overline{T}}{\partial y} + \overline{w}\frac{\partial \overline{T}}{\partial z}\right) = \frac{\partial}{\partial x}\left(\lambda\frac{\partial \overline{T}}{\partial x} - \rho C_P\overline{u'T'}\right) + \frac{\partial}{\partial y}\left(\mu\frac{\partial \overline{u}}{\partial y} - \rho C_P\overline{v'T'}\right)$$

$$+ \frac{\partial}{\partial z}\left(\mu\frac{\partial \overline{u}}{\partial z} - \rho C_P\overline{w'T'}\right) \qquad \text{(II. 10)}$$

By simulation we can write the extra temperature terms as a function of temperature gradient, as follows:

$$\overline{-\rho u'T'} = \Gamma_T\frac{\partial \overline{T}}{\partial x}; \overline{-\rho v'T'} = \Gamma_T\frac{\partial \overline{T}}{\partial y}; \overline{-\rho w'T'} = \Gamma_T\frac{\partial \overline{T}}{\partial z}; \qquad \text{(II. 11)}$$

Where: Γ_T is the turbulent diffusivity

Since the turbulent transport of momentum and heat is due to the same mechanisms, swirl mixing, the value of the turbulent diffusivity can be taken, to be close to turbulent viscosity. [16]

II.4 Numerical formulation:

II.4.1 Finite volume method:

The Finite Volume Method (FVM) is a numerical technique that transforms the partial differential equations representing conservation laws over differential volumes into discrete algebraic equations over finite volumes (or elements or cells). In a similar fashion to the finite difference or finite element method, the first step in the solution process is the discretization of the geometric domain, which in the FVM, is discretized into non-overlapping elements or finite volumes. The partial differential equations are then discretized/transformed into algebraic equations by integrating them over each discrete element. The system of algebraic equations is then solved to compute the values of the dependent variable for each of the elements.

In the finite volume method, some of the terms in the conservation equation are turned into face fluxes and evaluated at the finite volume faces. Because the flux entering a given volume is identical to that leaving the adjacent volume, the FVM is strictly conservative. This inherent conservation property of the FVM makes it the preferred method in CFD.

Another important attribute of the FVM is that it can be formulated in the physical space on unstructured polygonal meshes. Finally, in the FVM it is quite easy to implement a variety of boundary conditions in a non-invasive manner, since the unknown variables are evaluated at the centroids of the volume elements, not at their boundary faces.

These characteristics have made the Finite Volume Method quite suitable for the numerical simulation of a variety of applications involving fluid flow and heat and mass transfer, and developments in the method have been closely entwined with advances in CFD.

From a limited potential at inception confined to solving simple physics and geometry over structured grids, the FVM is now capable of dealing with all kinds of complex physics and applications.[18]

II.4.2 Boundary conditions:

The table II.1 shows the boundary conditions of this problem.

Table II.1: Boundary conditions

inlet	outlet	wall
Fluid Velocity(V_0) Fluid temperature(T_0)	pressure	The temperature at the walls (T_w)

II.4.3 Mesh independence:

The choice of the mesh is an essential step which influences the precision and the accuracy of the numerical results. Therefore, a mesh meeting the objectives, contains a number of stitches, a distance between the stitches and a shape of the stitch, suitable Practically, there are no precise rules for the creation of a mesh suitable, however there are different approaches that make it possible to obtain a grid acceptable, like:

- The maintenance of a good quality of the elements
- The assurance of good resolution in regions with strong gradients.
- The assurance of good smoothing in the transition zones between the parts to be fine mesh and those with coarse mesh.
- The minimization of the total number of elements (reasonable calculation time)

In general, the finer the finite element mesh, the more accurately one can capture the contours of a geometry and there are more "data points" on the geometry to generate an accurate displacement and stress response.

A mesh independence (or grid independence) study is something an analyst can perform to determine the dependence of the results on the mesh density.

Six cases of mesh are created to choose the optimal one table II.2. The water is used for this study; its physic characteristics are shown in Tab.II.2. The inlet velocity V0 equal to 0.308 m/s at (Re = 62472.95) and temperature (T0= 323 K). the wall temperature equal to 303 K.

Table II.2: Thermophysical characteristics of the water

Density (ρ)	998.2 kg/m3
Dynamic viscosity (μ)	0.001003 kg/m.s
Thermal conductivity (λ)	0.6 W/m.s
Heat capacity (Cp)	4182 g.K

Table II.3: Comparative table of proposed meshes.

MESH	Nbr of Nodes	Nbr of element	Initialization methods	Time
1	12343	29803	Hybrid	00:01:20
2	12343	29803	standard	00:00:53
3	21480	46667	Hybrid	00:01:57
4	21480	46667	standard	00:01:25
5	30864	65003	Hybrid	00:02:07
6	30864	65003	standard	00:01:28

(Fig II.4) shows the evolution of the velocity profile of the cases studied. The superposition of the velocity curves on top of each other means that the results have become independent of the mesh. In this case, the chosen mesh will be the one with the shortest execution time, with an inflation of the mesh near the walls to achieve smooth gradients. The mesh chosen was the second one.

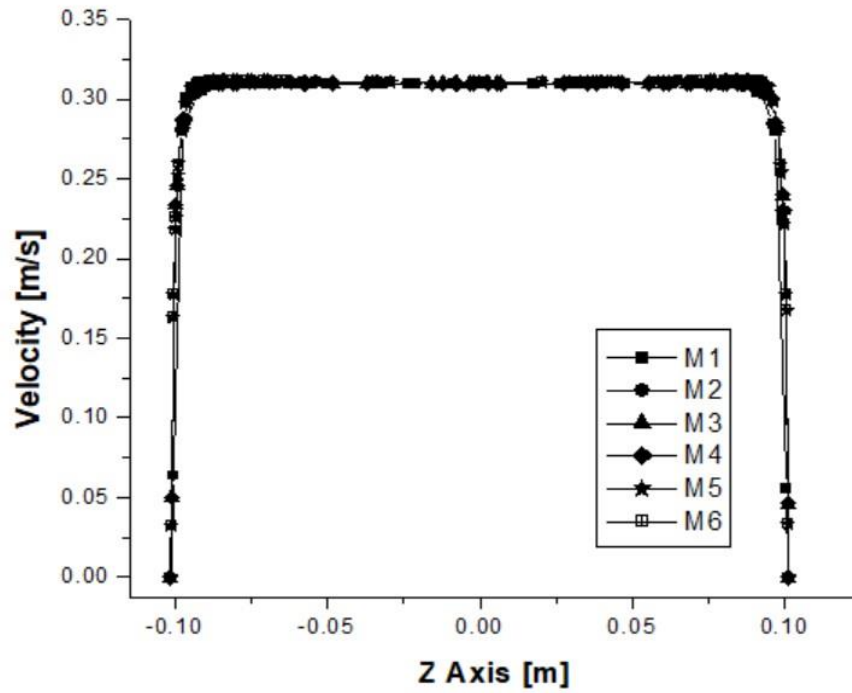(Fig II.5-6) show respectively the vertical projection and an overall 3-dimensional view of the chosen mesh.

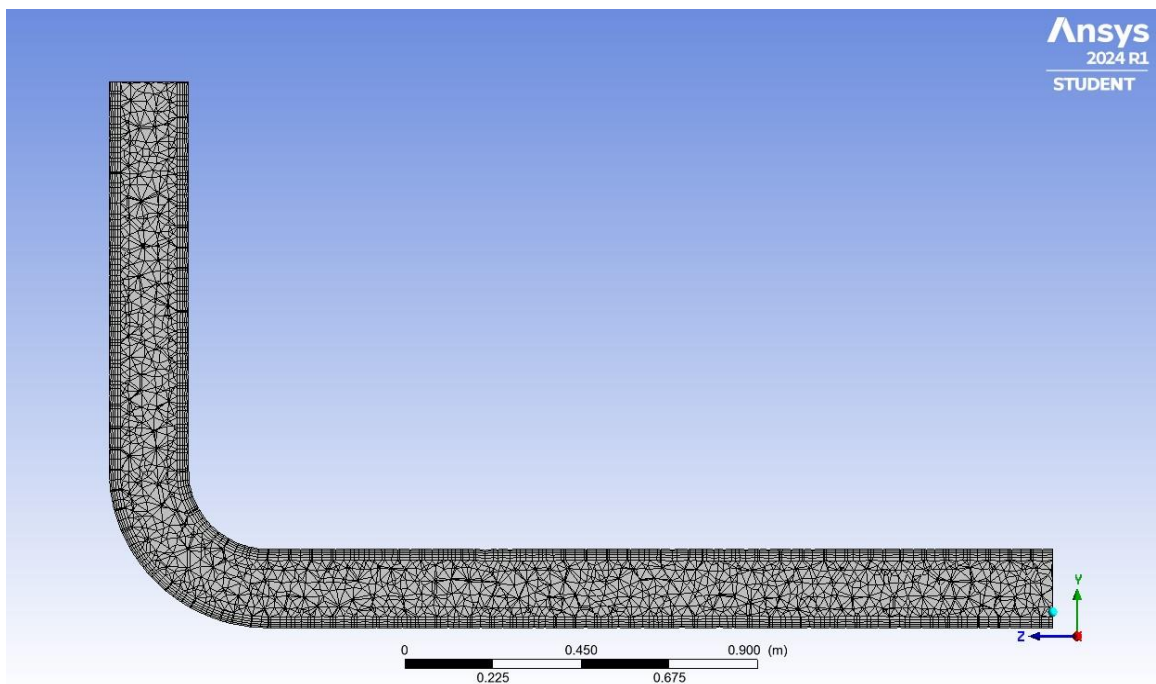Figure II.4: Velocity curves at the entrance of channel, Re = 62472.95
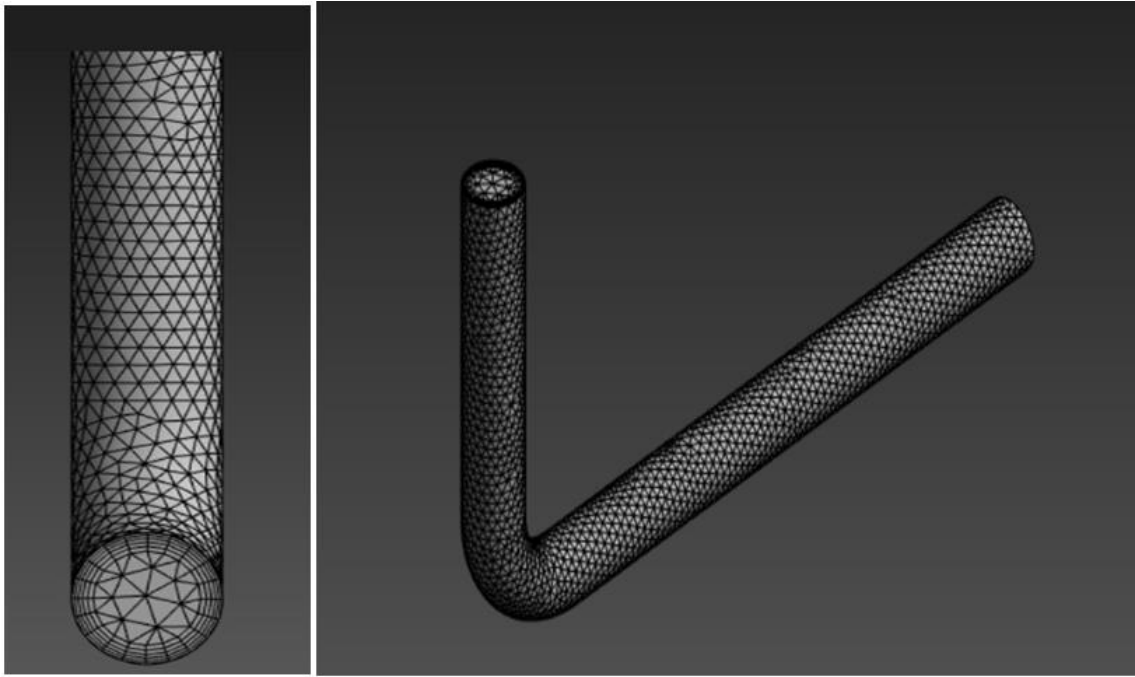

Figure II.5: Meh chosen, vertical projection

Figure II.6: Meh chosen, in 3 dimensions

CHAPTER III : RESULTS AND DISCUSSION

This chapter includes the results and discussions of the flow in a 90° elbow. The calculations are performed using the Ansys Fluent 24 code, based on the finite volume method to solve the energy balance established in the previous chapter.

III.1 Flow system conditioning:

The problem studied involves a steady, incompressible and forced flow within an elbow, using drilling mud as pseudoplastique fluid that follows the power-law. Its thermophysical characteristics, are mentioned in the table III.1

Table III.1: Thermophysical characteristics of the drilling mud

Density (ρ)	1030 kg.m^{-3}
Consistency index (K)	0.0577 kg.s (n^{-2}).m^{-1}
Flow index (n)	0.8549
Thermal conductivity (λ)	0.6 W.(m.s)$^{-1}$
Mass Specific heat capacity (Cp)	4070 J.(g.K)$^{-1}$

The Critical Reynolds number calculated for this study is equal to 2300, by the equation which are mentioned in chapter I. The flow regime studied in both laminar (Re = 1551) and turbulent (Re = 3430 and 5456). Its velocities at the inlet of the elbow are mentioned in Table.III.2. The inlet velocities were chosen based on the actual pumping speeds in an oilfield operation.

Table III 2: Regime flow conditions

	Case 1	Case 2	Case 3
Re	1551	3430	5456
V_0 [m.s^{-1}]	0.308	0.616	0.925
T_0 [K]	323	323	323
T_w [K]	303	303	303

The geometry of the elbow is mentioned in precedent chapter (§ II.2). This flow system is divided into several stations (eight lines), one in upstream of the elbow (L1), three within the elbow (L2, L3 and L4), and four in it downstream, each 40 centimetres

(L5, L6, L7 and L8). The elbow takes three positions as explained in the second chapter, Figure III.1.
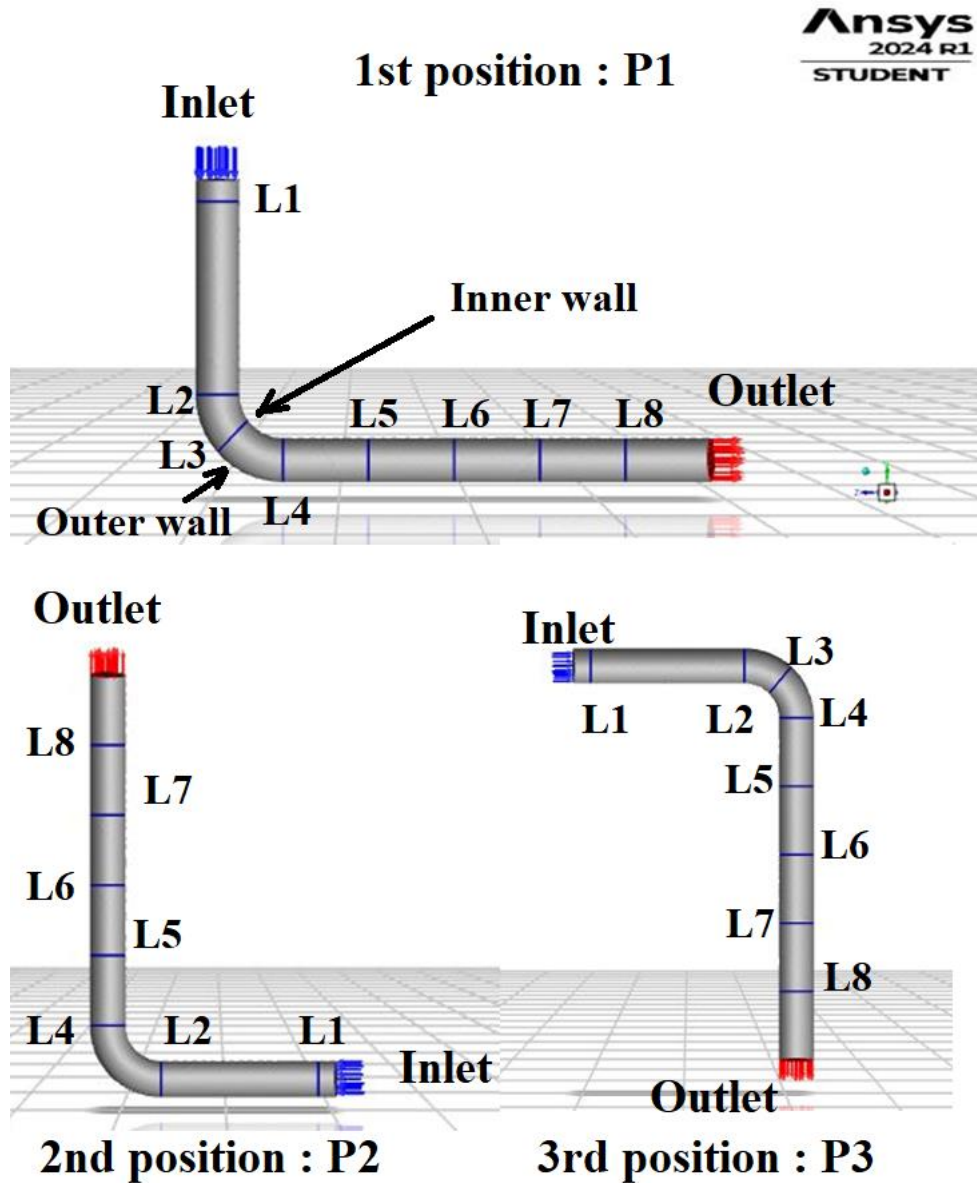

Figure III.1: Positions of elbow and stations studied

III.2 Results and discussions:

III.2.1   Velocity:

According to Figures III.2-4, its show that the appearance of the fluid and its velocity are almost the same. The noticeable difference concerns the flow direction, given the change in direction between the inlet and the outlet of the elbow, which justifies the

study of only one position. Therefore, the discussion of velocity is limited to the first position.
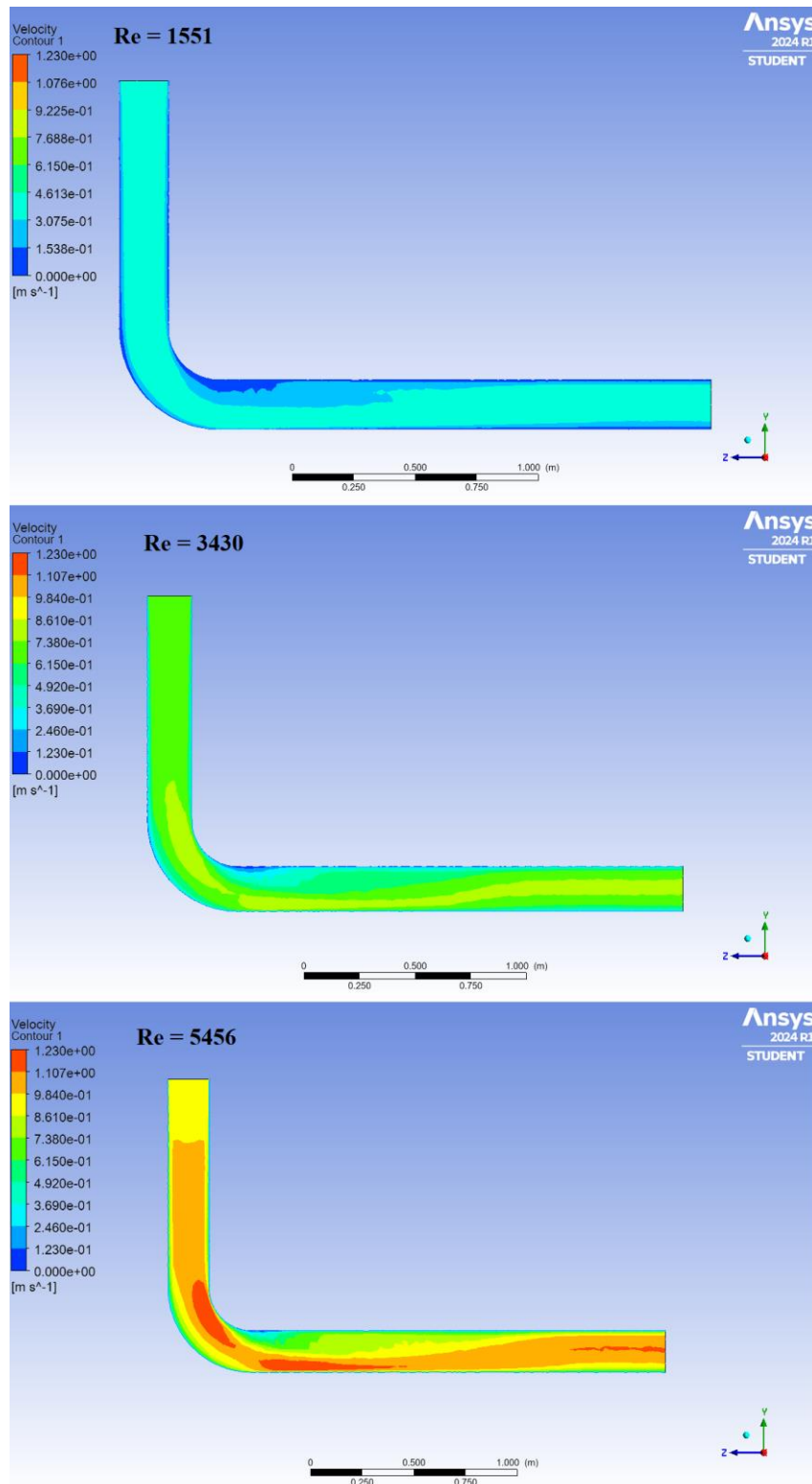
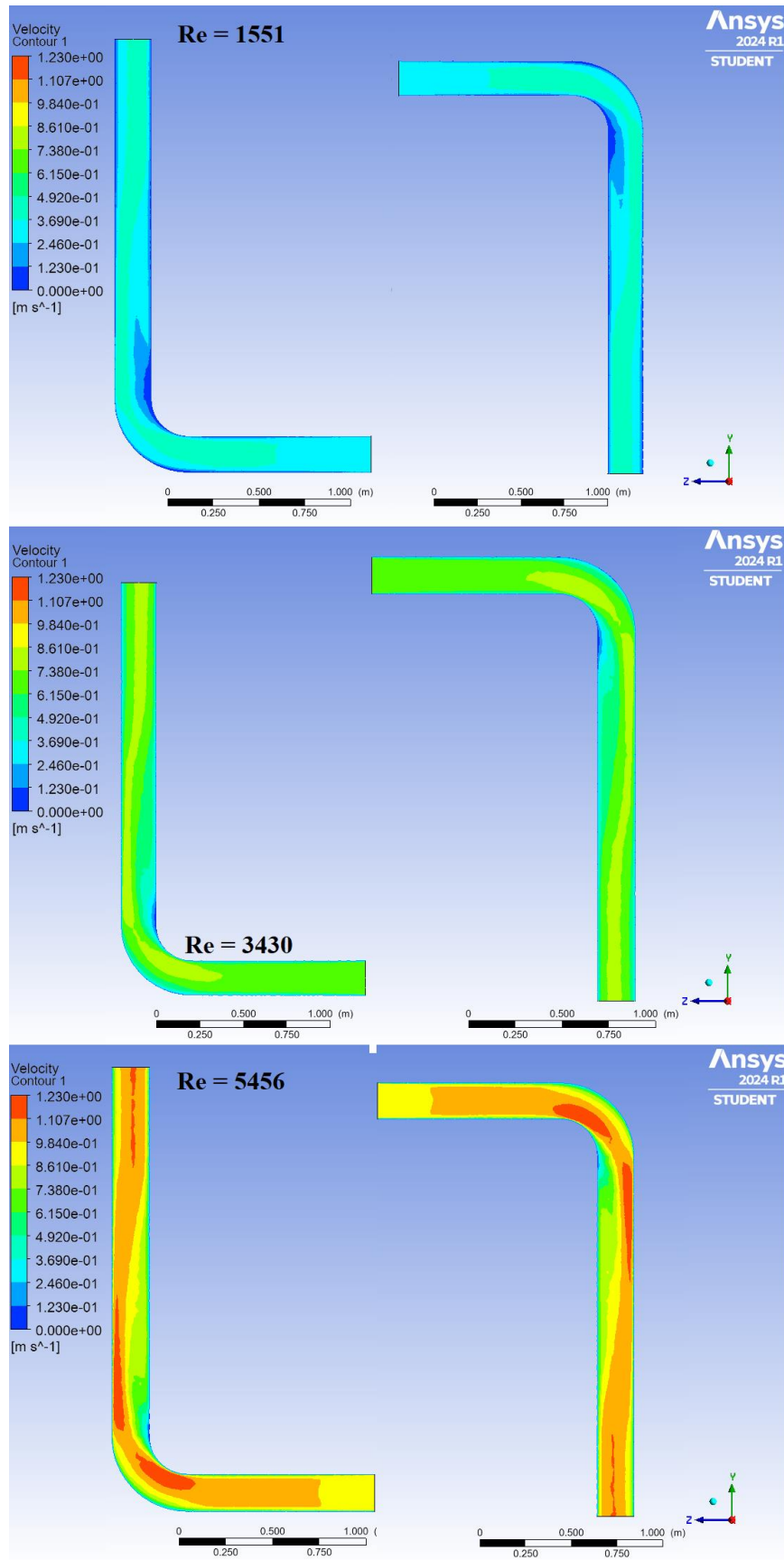Figure III.2: Velocity contours, 1st case

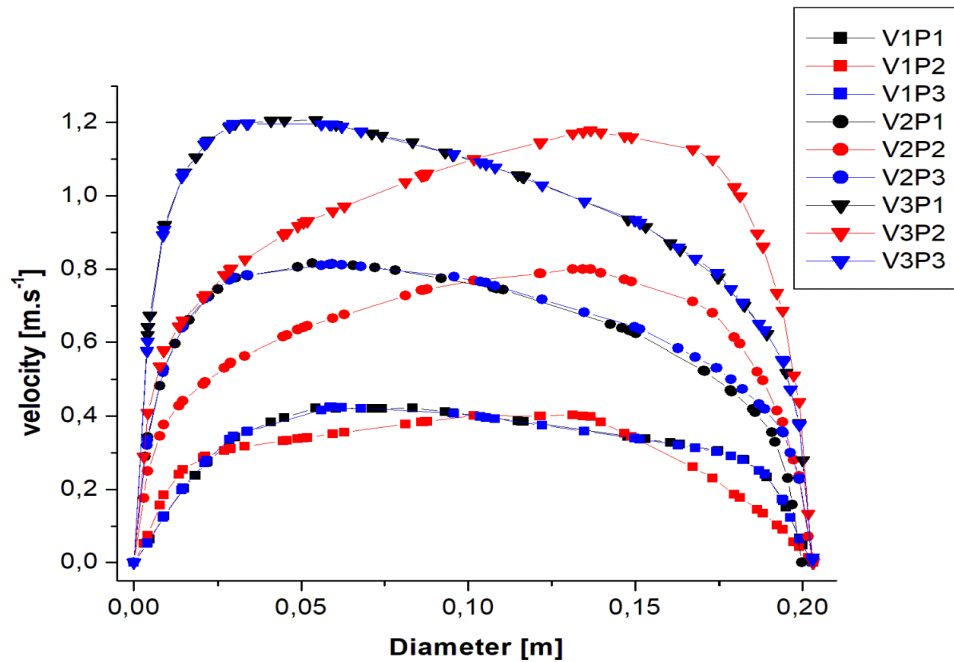Figure III.3: Velocity contours, 2nd case (in left), 3rd case (in right)

Figure III.4: Velocity in elbow, all positions, all Re

The flow at the entrance of the elbow differs considerably from a fully developed pipe flow. The flow in elbow is influenced by centrifugal force due to its curvature. [19] (Fig.III.5)

At the entrance of elbow, the more rapidly flowing central parts of the flow are forced outwards by centrifugal action, while the slower parts along the wall are forced inwards where the pressure is less, and a so- called "secondary flow" takes place at right angles to the main flow. If the curvature is significant, the axial velocity distribution is entirely altered by the secondary flow [20], (Fig.III.2, III.4-5). It is seen that the velocity profiles shift towards the inner side of the pipe.

The flow on the outer wall and separation at the inner wall make flow very complex. The result is a secondary flow superimposed in the main flow in the plane perpendicular to the main flow. The direct effect of secondary flow is to displace the region of maximum velocity to the centre towards the outer wall. [19]
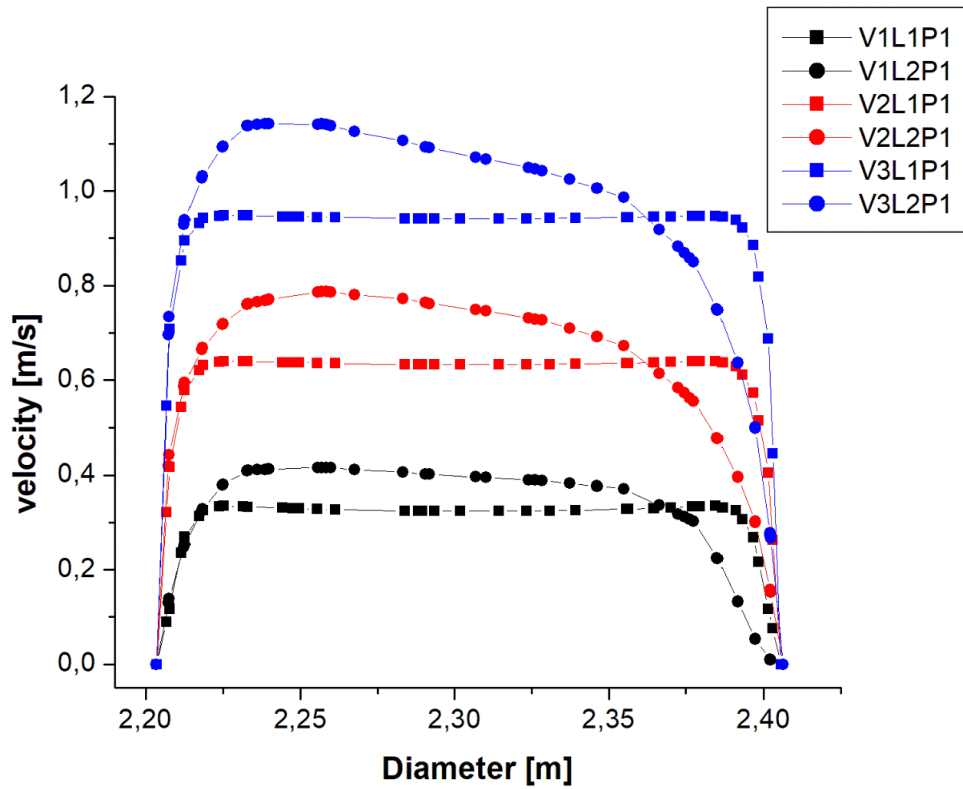
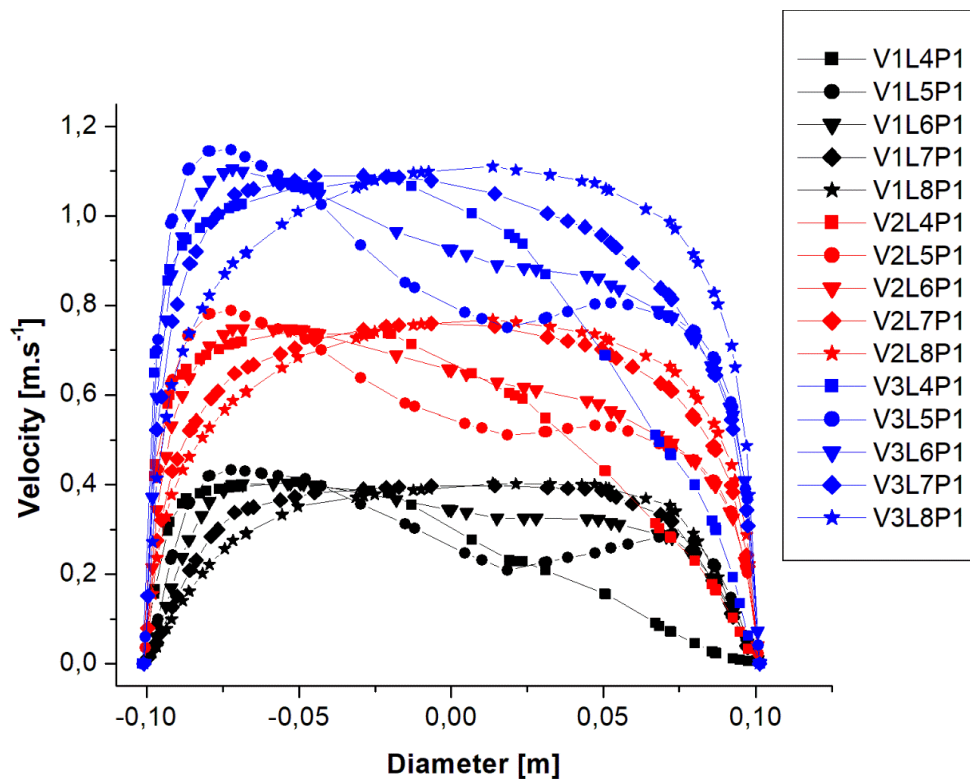Figure III.5: Upstream velocity in elbow, 1st position, all Re

Figure III.6: Downstream velocity in elbow, 1st position, all Re

The secondary flow which has been set up brings the fluid of large axial velocity from the outside to the inside, along the upper and lower walls. As a result, the fluid near the inner wall with small axial momentum shifts to the central portion of the pipe. [20]

The secondary flow attains its maximum intensity at the early stages of flow development, and further downstream, it weakens asymptotically until it becomes fully developed. For high Reynolds numbers, the separation of the secondary flow boundary layer near the inner wall is observed in the middle of the entry region, and it disappears at distances further downstream. The separation bubble thus formed may be the reason for the occurrence of the two-step plateaus in the axial flow development (Fig.III.2 and III.6) because it delays the transition to the fully developed state. The velocity profiles were found asymmetrical, with a movement towards the outsider pipe edge, when there was an increased Reynolds number. [21]

III.2.2   Temperature:

Figure III.7 indicates that centrifugal body forces have a strong influence on the heat transfer. Centrifugal body forces are weaker and the convective currents have strong influence on flow at low Reynolds number. The convex surface of the curved duct influences the flow and heat transfer more than the concave surface of the curved duct. [22] In turbulence, this region disappears.

III.2.3   Pressure:

At the inlet of the elbow a low pressure exists in the inner wall, at the inner wall nearest to the centre of curvature, and high pressure exists at the outer wall, at the outer wall furthest from the centre of curvature. This initial static pressure gradient resulting from the change from straight to curve flow, a cross stream pressure gradient exists in the elbow.

The reverse occurs at the exit of the elbow where local pressure gradients of the opposite sign appear as the flow adjust to uniform pressure condition of the downstream. [19]
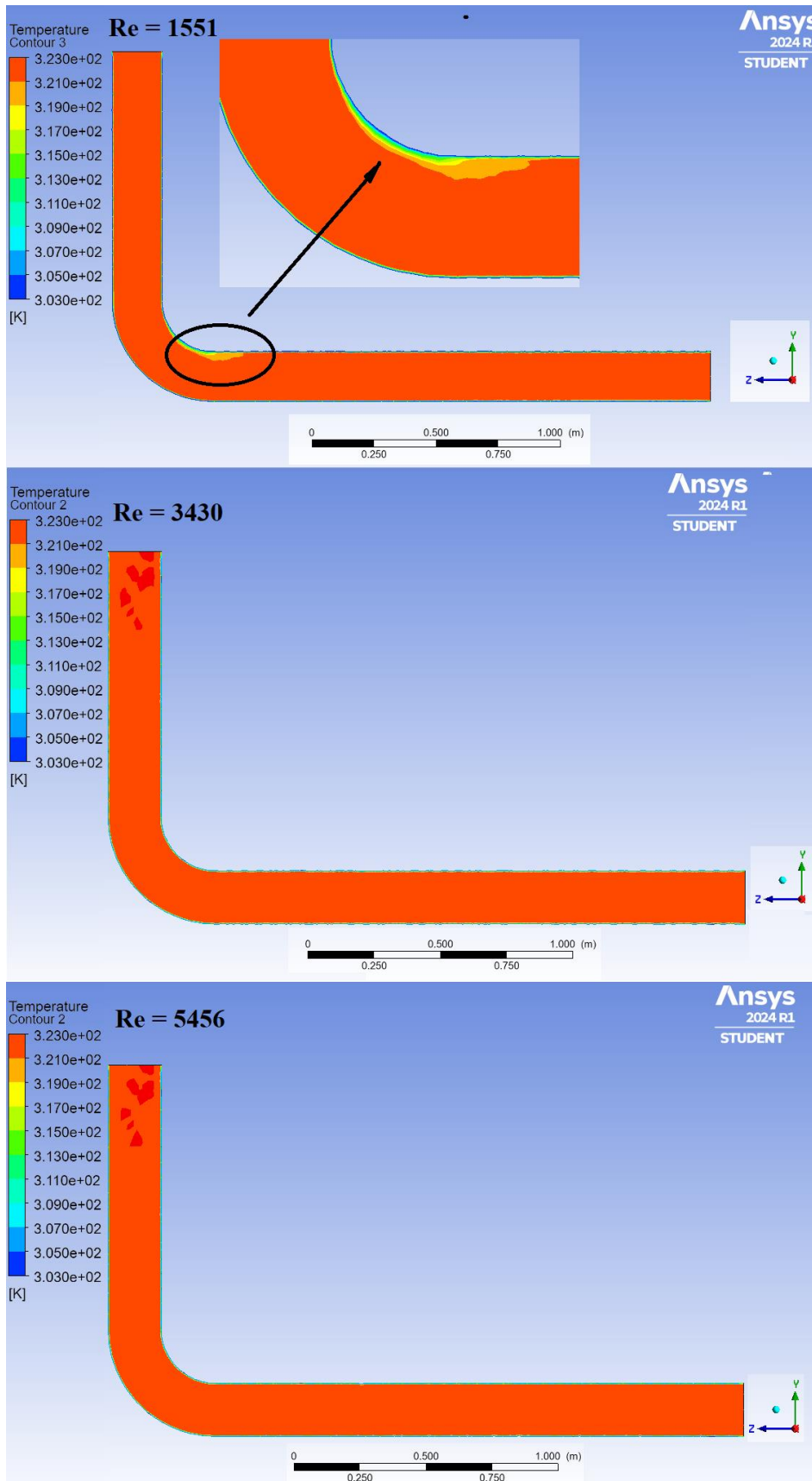
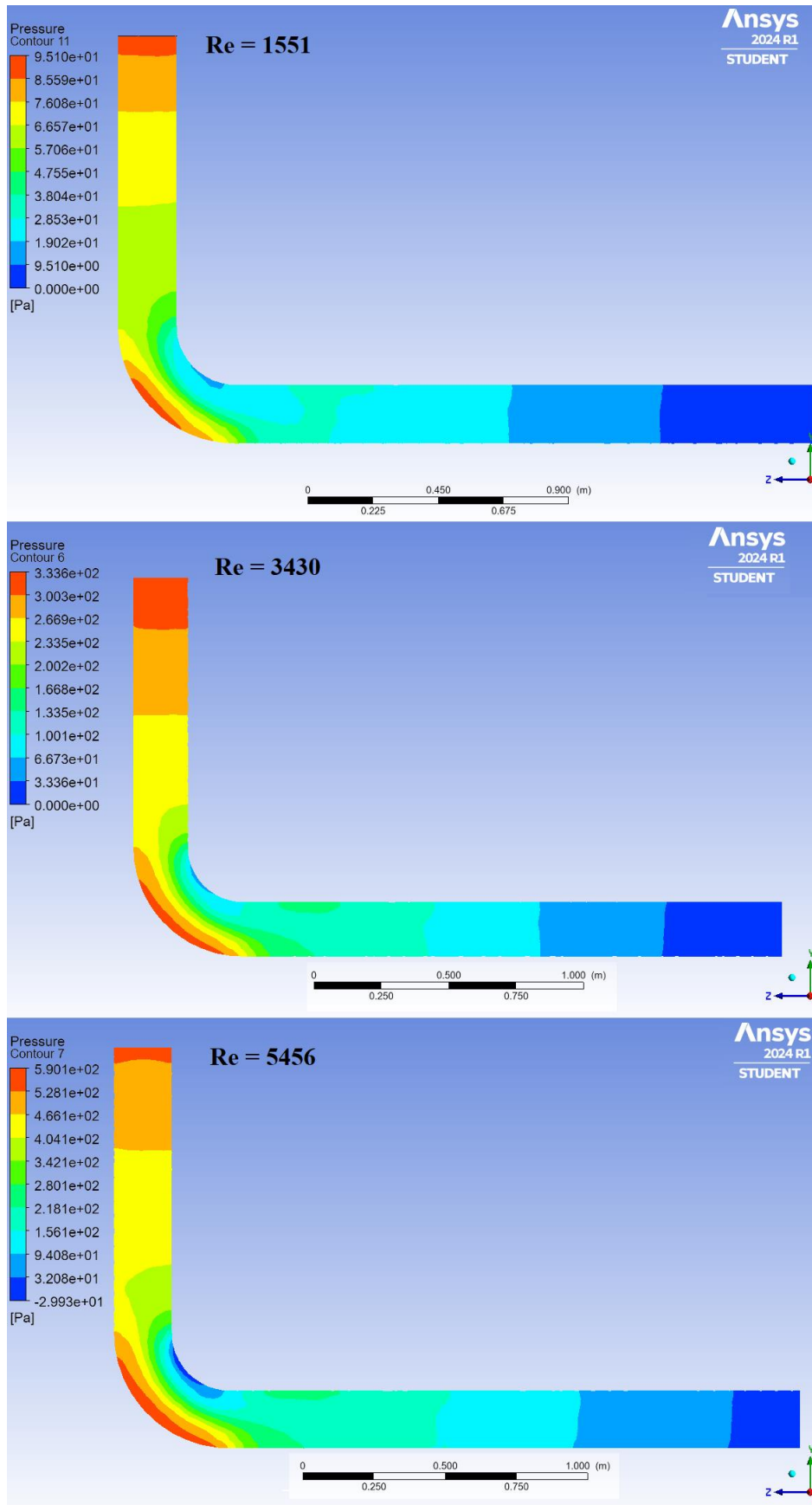Figure III.7: Temperature in elbow, 1st position, all Re

Figure III.8: Static pressure in elbow, 1st position, all Re

At the inner bend wall, separation of the boundary layer with subsequent formation of secondary circulation currents took place resulting in a low value of the recorded pressure in this region. Stagnation points have been observed in both of these regions.

The static pressure is proportional to the Reynolds number; it clearly increases with the rise in Re. The pressure gradient in the bend between the two walls also becomes more pronounced, which affects the fluid velocity. (Fig.III.8)

III.2.4 Pressure drop:

The pressure losses suffered in a bend are caused by both friction and momentum exchanges resulting from a change in the direction of flow. Both these factors depend on the bend angle, the curvature ratio and the Reynolds Number. The overall pressure drop can be expressed as the sum of two components, resulting from friction in a straight pipe of equivalent length which depends mainly on the Reynolds number (and the pipe roughness); and that resulting from losses due to change of direction, normally expressed in terms of a bend-loss coefficient, which depends mainly on the curvature ratio and the bend angle. [6]

In the first chapters, several equations are established to calculate head losses and their coefficients, generally for Newtonian fluids (I.15, I.19-22 and I.27-29) and particularly for pseudoplastic fluids (I.16-18). In this section, a comparison between these equations is made to see the influence of the fluid type on the pressure drop and the suitability of the equations to represent these losses.

The loss pressure is greatly affected by the flow regime and the length of the downstream tangent, as shown in Figure III.9. The influence of the Reynolds number on head losses is significant; there is a proportionality between them. Figures III.10–11 show that, at the entrance and the middle of the bend, at low Re (laminar flow), the pressure drops are almost the same when applying both equations, as the fluid in these two lines has not yet changed direction and the pressure gradient between the lower and upper walls of the bend is low. However, a significant discrepancy is noticeable between the

application of the two equations as Re increases, implying that the equation has a mutual relationship with the type of fluid.
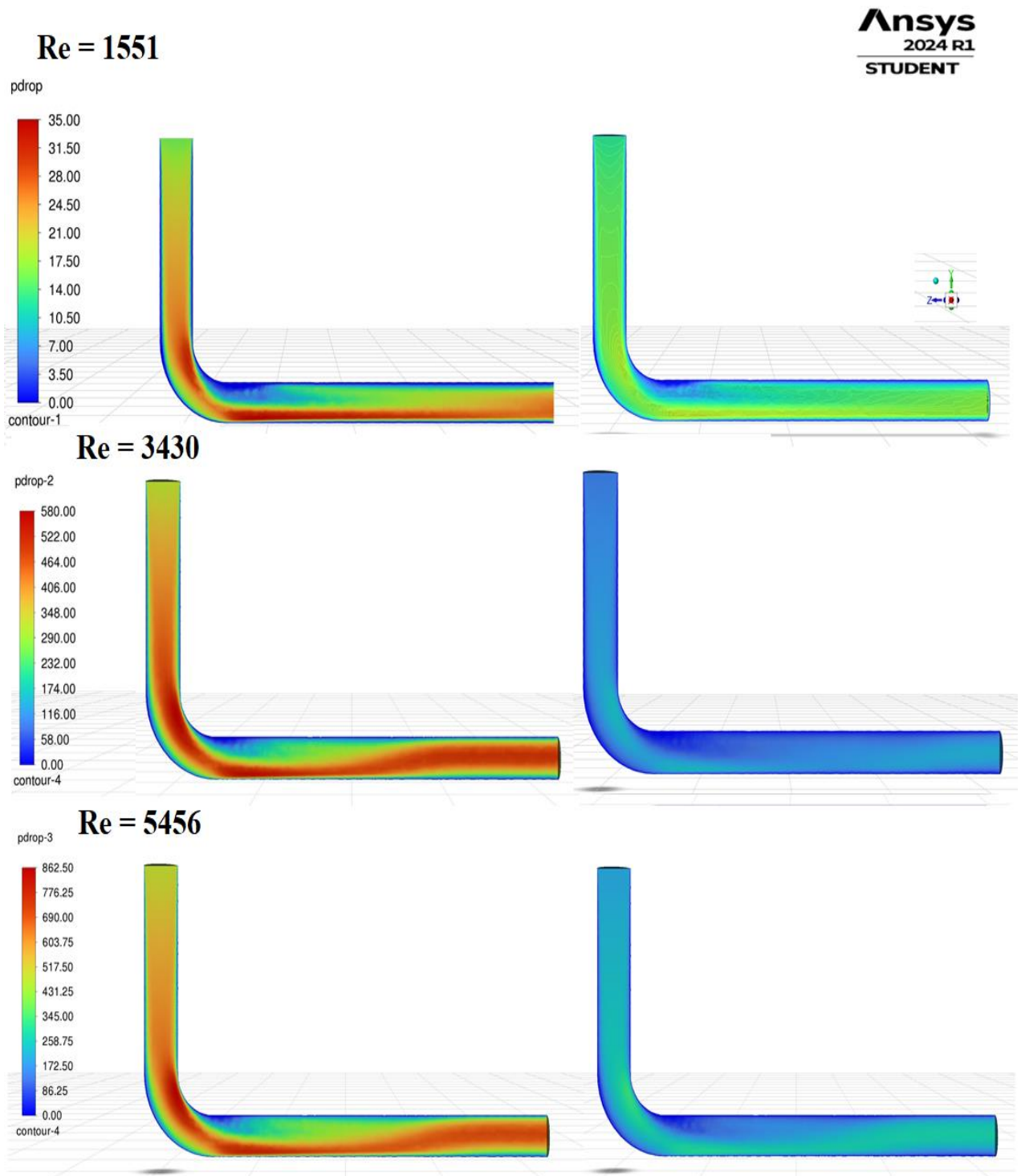

Figure III.9: Pressure drop, all Re, in left Newtonian equation , in right non Newtonian equation
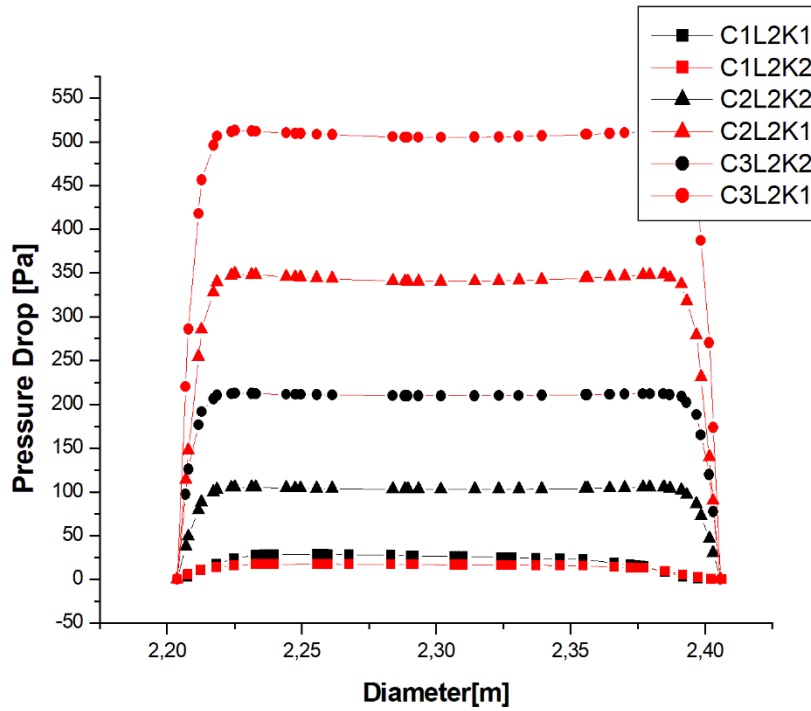
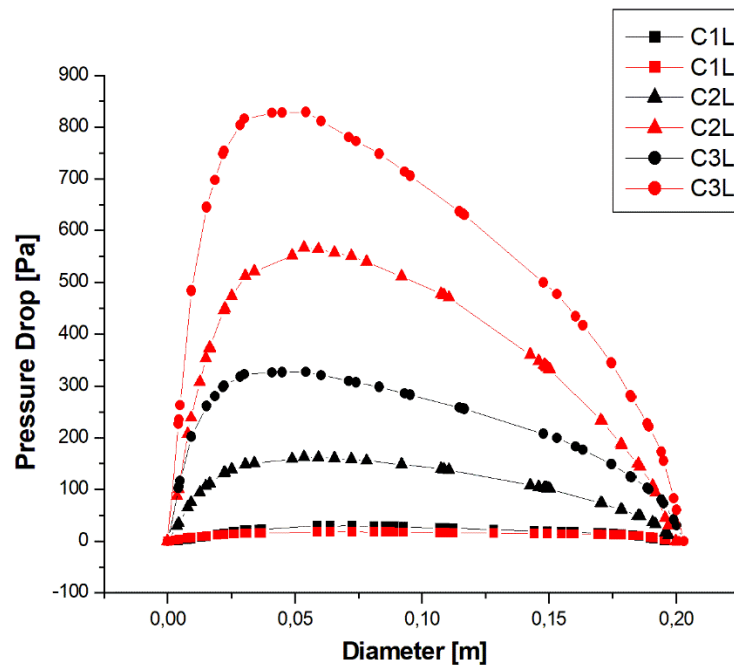Figure III.10: Pressure drop at the inlet of elbow, all Re, all equations

Figure III.11: Pressure drop at the middle of elbow, all Re, all equations

Figures III.12–14 show a significant discrepancy downstream of the bend and sometimes changes in the shapes of the curves where the fluid has changed direction, along with the presence of flow reversal, creating zones where it temporarily stagnates. All these anomalies affect the type of fluid used, implying the necessity of applying the correct equation in the right location. These figures also ensure the proportionality between pressure losses and the Reynolds number.
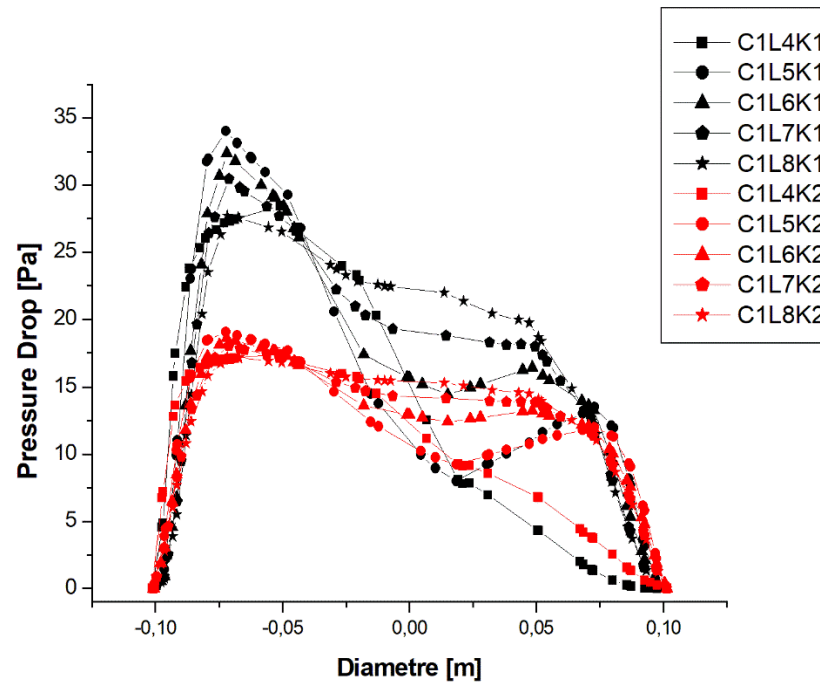

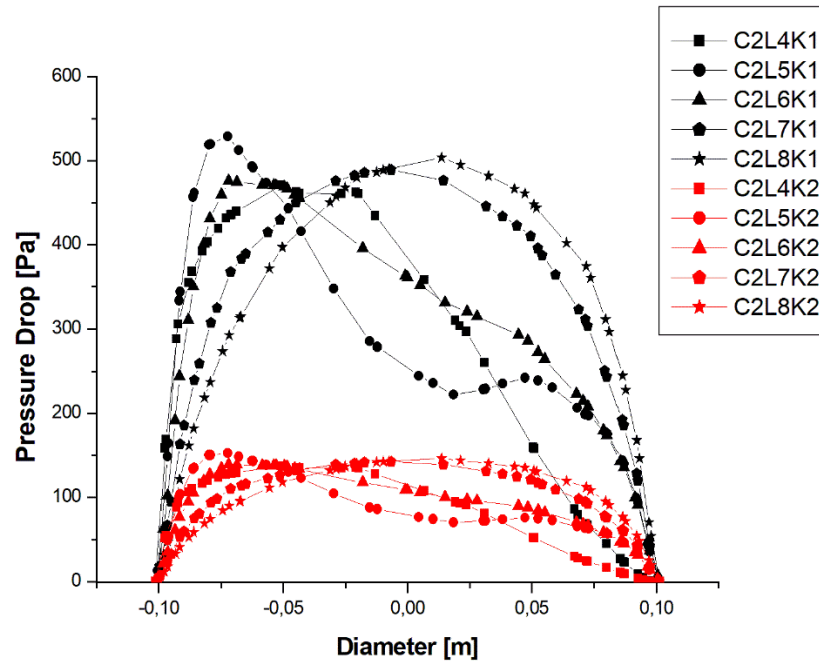Figure III.12: Pressure drop at the outlet and downstream of elbow, Re = 1551, all equations

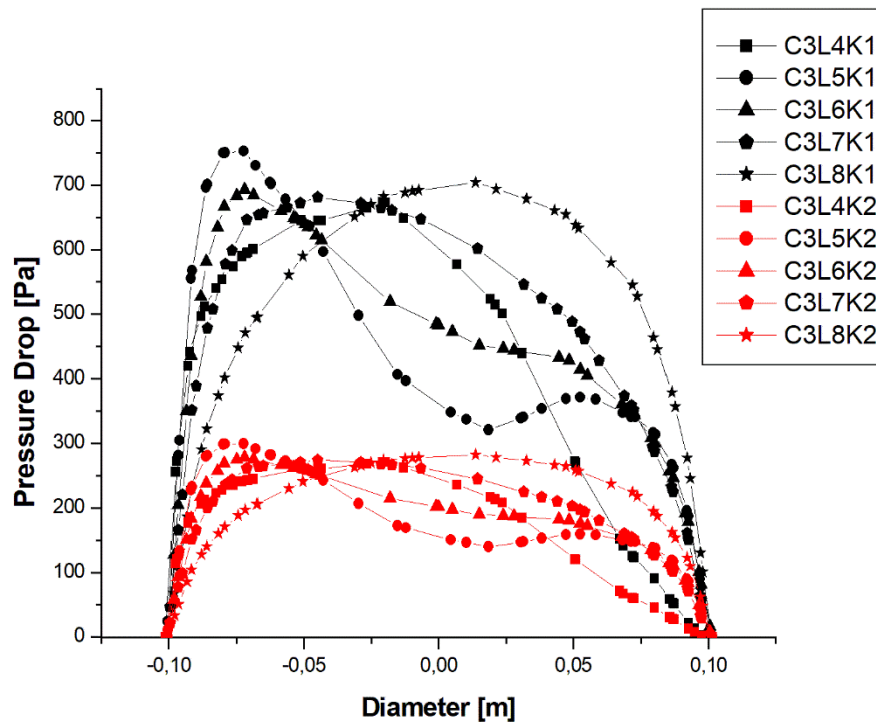Figure III.13: Pressure drop at the outlet and downstream of elbow , Re = 3430, all equations

Figure III.14: Pressure drop at the outlet and downstream of elbow, Re = 5456, all equations

CONCLUSION

This work studied the steady, forced, and incompressible flow in the 90° elbow-long radius using pseudoplastic non-Newtonian fluid, obeyed by the power law, in a laminar and turbulent regime.

The conclusion can be summarized at the next point:

- As soon as the flow enters the elbow, the velocity profile becomes irregular, and when it moves inside the elbow, the maximum velocity tends to occur gradually towards the outer wall of the elbow. Near the outlet section, this maximum velocity occurs fully at the outer wall, which is due to the effect of curvature.

- The position of the bend does not influence the flow regime or velocity profile; the only change concerns the direction of flow.

- The static pressure contour on the symmetry plane shows higher pressure on the outer side of the bend, corresponding to lower velocity in that region. The area of low pressure on the inner bend side is associated with the flow separation regions.

- The pressure gradient within the bend between the two lower and outer walls produces pressure drops.

- The pressure drops in and downstream of the bend are proportional to the Reynolds number.

- The equation for calculating these losses must be suitable for the type of fluid.

The recommendations to continue this research are:

- Study the effect of the pressure coefficient.

- Investigate other types of bends, such as 45° and 180° bends.

[1] Don W. Green, Robert H. Perry, Perry's Chemical Engineers' Handbook, 8th Edition, McGraw-Hill Companies, Inc, 2008

[2] Trade Union Chamber of Research and Production of Petroleum and Natural Gas Committee of technicians, Drilling Mud and Cement Slurry Rheology, Springer Science & Business Media,1982

[3] K.V. Chandrasekharm, Introduction to Fluids in Motion: University Guntur, India: international Journal on Recent and Innovation Trends in Computing and Communication, 2017

[4] R.P. Chhabra, J.F. Richardson, Non-Newtonian flow and applied rheology: engineering applications, 2nd edition, ICHEM, 2008

[5] Exlog Staff , Alun Whittaker,1985: Theory and Application of Drilling Fluid Hydraulics, The EXLOG Series of Petroleum Geology and Engineering Handbooks.P68.

[6] F. A. Holland and R. Bragg, Fluid Flow for Chemical Engineers, 2nd edition, ARNOLD A member of the Hodder Headline Group, 1995

[7] Ron Darby, chemical engineering fluid mechanics, 2nd edition, Marcel Dekker, Inc, 2001

[8] 'Perte de charge pour les systèmes de ventilation industrielle', Wattohm. Perte de charge pour les systèmes de ventilation | Wattohm,19/05/2024, 10h pm

[9] 'Pressure Loss in Pipe | Neutrium'. Accessed: May 19, 2024. [Online]. Available: https://neutrium.net/fluid-flow/pressure-loss-in-pipe/

[10] PHILIP J. PRITCHARD, JOHN C. LEYLEGIAN, Fox and McDonald's Introduction to fluid mechanics, 8th edition, JOHN WILEY & SONS, INC, 2011

[11] White, Frank M. FLUID MECHANICS, SEVENTH EDITION Published by McGraw-Hill, 2011

 [12] https://www.continental-steel.com/Pipe-fitting/pipe-fitting-elbow.html, 18/05/2024 20H

[13] https://www.growmechanical.com/what-is-pipe-elbow/18/05/2024 20H

[14] https://whatispiping.com/piping-elbows-and-bends/ 18/05/2024 20H

[15] DONALD C. RENNELS, HOBART M. HUDSON, PIPE FLOW: A Practical and Comprehensive Guide, First Edition. Inc. Published 2012 by John Wiley & Sons, Inc .

[16] Sal Rodriguez, Applied Computational Fluid Dynamics and Turbulence Modeling Practical Tools, Tips and Technique, Springer, 2019

[17] https://www.simscale.com/docs/simulation-setup/global-settings/k-epsilon/.

[18] F.Moukalled & L.Mangani & M.Darwish: January 2015: The Finite volume method in computational fluid dynamics.

[19] T. K. Bandyopadhyay, S. K. Das, Non-Newtonian and Gas-non–Newtonian Liquid Flow through Elbows – CFD Analysis, Journal of Applied Fluid Mechanics (JAFM), Vol. 6, No. 1, pp. 131-141, 2013.

[20] Hidsato Ito, Flow in curved pipe, JSME International Journal, Vol 30, No 262, 1987

[21] Asterios Pantokratoras, Steady laminar flow in a 90° bend, Advances in Mechanical Engineering, Vol. 8(9), pp 1–9, 2016

[22] Rajesh Kumar Ojha, P. V. Joshi, Numerical Analysis of Forced Convection and Heat Transfer in Curved Duct, International Journal of Recent Trends in Mechanical Engineering (IJRTME), Vol. 2, Issue. 4, June. 2014